Planetary and Space Science 219 (2022) 105515

Contents lists available at ScienceDirect

Planetary and Space Science

journal homepage: www.elsevier.com/locate/pss

CaSSIS-based stereo products for Mars after three years in orbit

Cristina Re [a,*], Audrie Fennema [b], Emanuele Simioni [a], Sarah Sutton [b], Daniel Mège [c], Klaus Gwinner [d], Mateusz Józefowicz [e], Giovanni Munaretto [a], Maurizio Pajola [a], Amedeo Petrella [a], Antoine Pommerol [f], Gabriele Cremonese [a], Nicolas Thomas [f]

[a] INAF-Astronomical Observatory Padova, Padova, Italy
[b] Lunar and Planetary Laboratory, University of Arizona, 1541 E. University Blvd, Tucson, AZ, 85721-063, USA
[c] Centrum Badań Kosmicznych Polskiej Akademii Nauk, Bartycka 18A, 00-716, Warszawa, Poland
[d] Institute of Planetary Research, German Aerospace Center (DLR), Rutherfordstr. 2, D-12489, Berlin, Germany
[e] Mateusz Józefowicz, European Space Foundation, Cracow, Poland
[f] Physikalisches Institut,University of Bern, Sidlerstr. 5, 3012, Bern, Switzerland

A B S T R A C T

The Colour and Stereo Surface Imaging System (CaSSIS) on board the ExoMars Trace Gas Orbiter (TGO), operating in push-frame mode, provides multiband images at four different wavelengths thanks to a Filter Strip Assembly with a panchromatic filter and three broadband filters within the visible and near infrared range. The camera acquires stereo pairs fundamental for the initialization of the photogrammetric process to perform three-dimensional reconstruction of the Martian surface at the best resolution of 4.6 m per pixel for regions up to ~400 km^2 in one imaging sequence.

The 3D points derived from the stereo processing are used to generate Digital Terrain Models (DTMs) with height accuracy on the order of one image pixel on ground allowing high-resolution morphometric studies and in general improving the understanding of the geology and geomorphology of the surface of Mars.

This work provides a review of the CaSSIS stereo products supported by a description of the applied methods and examines some specific approaches directed to science analysis. Furthermore, our development of methods is herein focused on the proof of concept and the performance of our dedicated pipeline. The DTM generation procedure has been implemented in a stereo photogrammetric pipeline by the team of the National Institute for Astrophysics-Astronomical Observatory of Padova (INAF-OAPd). The workflow is based on area-based image matching integrated in a multi-resolution approach where the quality of the image matching largely determines the quality of the output DTM. For this reason, the influence of the parameters involved in the matching process (i.e. number of tie-points, template sizes and shape models in matching) has been studied.

CaSSIS stereo products have been generated for approximately 0.1% of the surface of Mars and 16.3% of the total stereo images acquired so far. In this work, some scientifically interesting targets have been considered in the investigation to provide an overview of the quality of the stereo results.

The experimental studies related to stereo analysis frequently led to comparison tests since they represent the best approach for contributing to the methodological consolidation of the photogrammetric data processing. The quality assessment based on comparison with reference terrain data is very promising also in considering areas with different surface type and morphologies.

1. Introduction

The Colour and Stereo Surface Imaging System (CaSSIS) (Thomas et al., 2017) with its stereo capabilities was conceived for enhancing our knowledge of the surface of Mars by extending and complementing the observations of previous instruments such as the High Resolution Imaging Science Experiment (HiRISE) (McEwen et al., 2007) which is currently operating on board NASA's Mars Reconnaissance Orbiter (MRO). Even before, other systems have imaged the surface of Mars in stereo mode. The High Resolution Stereo Camera (HRSC) (Neukum and Jaumann, 2004) (Jaumann et al., 2007); of the Mars Express mission was one of the first stereo camera designed to derive digital terrain models (DTMs) and the corresponding orthoimages on its standard operation mode with resolution better than 20 m/pixel. Furthermore, the Context Camera (CTX (Malin et al., 2007)), for other MRO observations, is able to acquire stereoscopic image pairs with imaging scale similar to CaSSIS (~6 m/pixel) operating in push broom mode. Both HiRISE and CTX acquire stereo pairs thanks to the ability of MRO to point off-nadir such that the camera can be pointed at specific targets.

CaSSIS adopts a single focal plane with four fixed colour filters and is able to acquire along-track stereo images thanks to a rotation mechanism. In the push-frame approach, the 2D image (hereafter called "framelet") is acquired, then buffered, read while the spacecraft moves and transferred to the proximity electronics before the next framelet is acquired,

* Corresponding author.
E-mail address: cristina.re@inaf.it (C. Re).

https://doi.org/10.1016/j.pss.2022.105515
Received 9 April 2021; Received in revised form 17 January 2022; Accepted 17 May 2022
Available online 30 May 2022

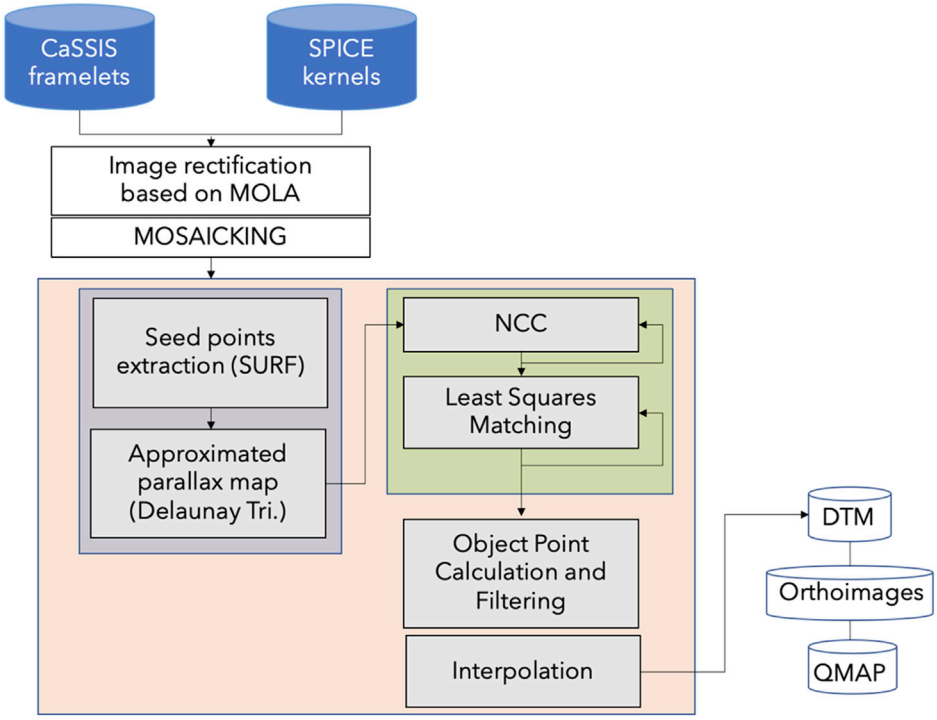

Fig. 1. Block diagram of the processing chain from the Images data (Framelets) and SPICE kernels to the products.

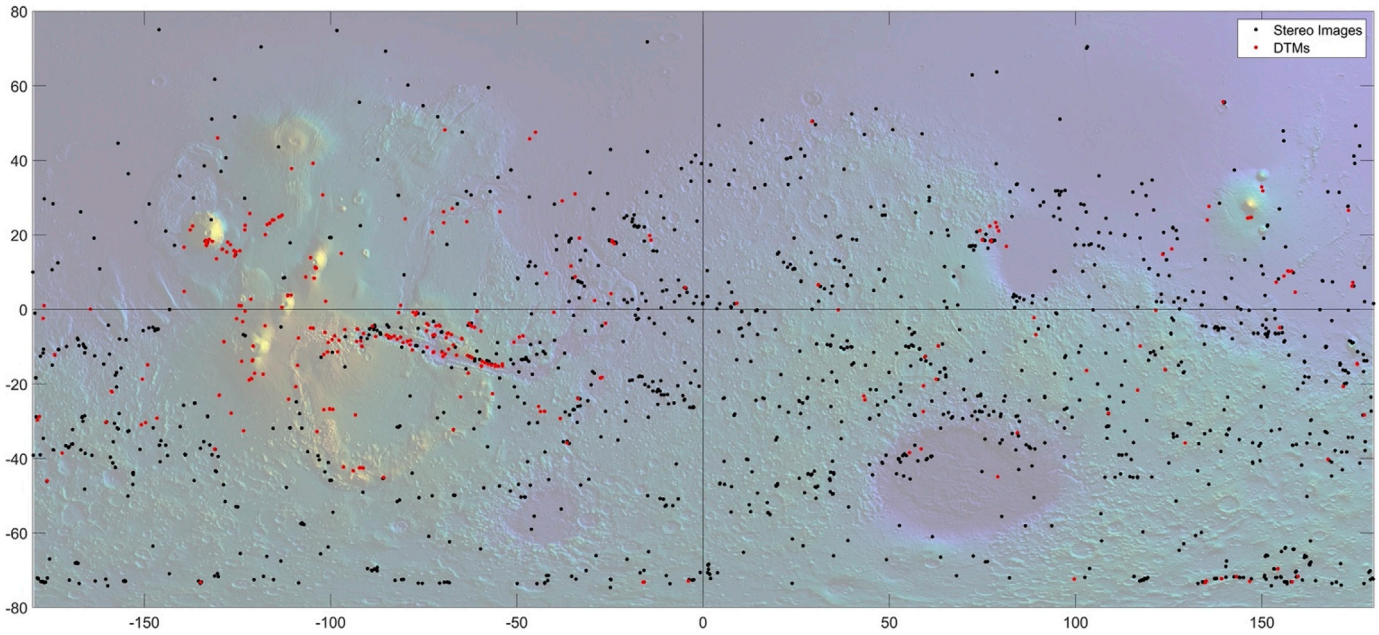

Fig. 2. Map of all the targets acquired by CaSSIS in stereo mode through MTP-29 (with different filters combinations) on the MOLA height map (black dots). Red dots show the DTMs reconstructed by 3DPD pipeline and available from the website Repository.

considering a sufficient surface overlap with the previous one. In the moving of the spacecraft along the orbit, CaSSIS acquires push-frame images to build up a full image swath (first of the pair) before rotating by 180°, thanks to a rotational stage, to acquire the second image of the pair. The telescope, furthermore, is mounted tilted by 10° with respect to the mechanical axis of symmetry of the bearing (nadir direction) guaranteeing a stereo convergence angle of 22.4° for a circular orbit at a height of around 400 km above Mars surface.

CaSSIS is the most recent example of a stereo camera employed in the photogrammetric mapping for planetary exploration. The processing techniques described here, applied to the imaging data, allow us to derive high-level stereo products such as the high-resolution DTMs, the corresponding orthoimages and anaglyphs. The expectations on the CaSSIS data are to provide stereo coverage over the surface equivalent to ~1–2% of the planet for every Martian year in orbit, complementing the other stereo data in terms of high resolution, colour and 3D mapping. The availability of three-dimensional data of a planetary surface enables the quantitative morphological analysis of any particular features, such as

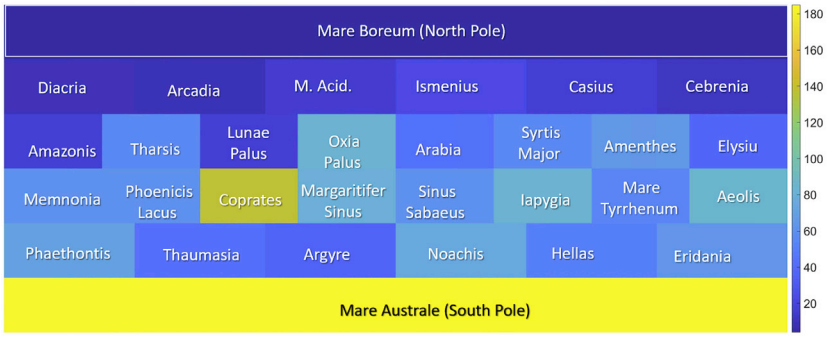

		Number of Stereo Couple
MC-01	Mare Boreum (North Pole)	4
MC-02	Diacria	10
MC-03	Arcadia	9
MC-04	Mare Acidalium	16
MC-05	Ismenius Lacus	22
MC-06	Casius	17
MC-07	Cebrenia	12
MC-08	Amazonis	17
MC-09	Tharsis	56
MC-10	Lunae Palus	17
MC-11	Oxia Palus	83
MC-12	Arabia	43
MC-13	Syrtis Major	57
MC-14	Amenthes	66
MC-15	Elysiu	38
MC-16	Memnonia	61
MC-17	Phoenicis Lacus	61
MC-18	Coprates	137
MC-19	Margaritifer Sinus	80
MC-20	Sinus Sabaeus	61
MC-21	Iapygia	83
MC-22	Mare Tyrrhenum	54
MC-23	Aeolis	84
MC-24	Phaethontis	71
MC-25	Thaumasia	43
MC-26	Argyre	37
MC-27	Noachis	75
MC-28	Hellas	51
MC-29	Eridania	63
MC-30	Mare Australe (South Pole)	185

(a) *(b)*

Fig. 3. In (a) the distribution of the stereo pair acquired by CaSSIS through MTP (Medium Term Plan) 29 divided in quadrangles. In (b) the same data reported as a numerical table. (the TGO's orbit does not allow CaSSIS to image at the poles).

impact crater interiors and their ejecta blankets, the volcanic domes, mountain chains or hills, mounds, drainage divides, as well as incised or inverted riverbeds and deltas.

More specifically, CaSSIS DTMs and orthoimages have been already used to investigate the stratigraphy of the South Polar Layered Deposits (Becerra et al., 2019). In addition, they have been used to perform the topographic correction on CaSSIS orthoimages (i.e., modeling and removal of brightness differences induced by topography), allowing to obtain corrected images that will be key for future photometric analyses of Maritan surface features (Munaretto et al., 2021).

The ability of CaSSIS to acquire along-track stereo, near-simultaneous stereo pairs avoids illumination differences between images and offers benefits for the DTMs and anaglyphs production.

This is especially beneficial since the orbit of TGO precesses through all local times of the day (Beta angle), and revisit times are much farther apart (depending on latitude) than those of MRO, which is in a Sun-synchronous orbit, but acquires stereo pairs on different orbits. In this paper, a description of these CaSSIS stereo products is proposed with particular attention to the effect of input parameters on the quality and precision of the DTMs. In the photogrammetric processing section, the general procedure is described and a series of different processing parameters is applied to test several strategies driven by the scientific investigation scope. The variability of the input data (image content and textures related to the illumination conditions and morphologic characteristics) suggests the application of flexible processing parameters for the derivation of highly accurate DTMs. The quality of the products has been assessed in terms of internal accuracy in terms of completeness of the surface, details of the reconstructed surface shape and morphologic consistency. The results are compared with DTMs provided by other Mars imagers (HiRISE and CTX). In order to extract robust statistics and to be able to derive considerations from the comparison a co-registration process between the datasets has been fundamental.

The paper is organized as follows. Section 2 describes the photogrammetric processing implemented in the OAPD-INAF pipeline (3DPD software). In Section 3, the CaSSIS stereogrammetric products are described and in Section 4 the anaglyph processing is presented. Section 5 elaborates the methodology and describes the experimental dataset. In Section 6, the performance analysis of the photogrammetric products is reported in details, and is also supported also by qualitative analysis. A final discussion and conclusions are provided in Section 7.

2. Photogrammetric processing

The Observatory of Padova team (OAPD-INAF) 3DPD pipeline (Simioni et al., 2021) is currently generating stereo data products (DTMs and orthoimages) from the CaSSIS images. All the data are delivered to a dedicated repository accessible through a web-interface (https://cassis.oapd.inaf.it/*archive*) (Cremonese et al., 2018) that is designed to manage the distribution of the DTMs (and connected ancillary products) within the CaSSIS team. The system provides on-line visualization and permits the download of the stereo products delivered periodically after their validation, managing also the query of the DTM to be generated. The single archive offers the benefits of having all the stereo data products from CaSSIS at one place, providing easy data accessibility to the entire team, as well as to entire Martian community, for geomorphological studies.

The photogrammetric pipeline proposed by the OAPD-INAF, described in details in (Simioni et al., 2021), contains automatic procedures for the creation of rectified mosaics from the framelets, definition of an initial disparity map for the disparity refinement at the sub-pixel level using a pyramid-based least-squares correlation process and finally for the triangulation phase and DTM production through raster interpolation (Fig. 1).

The OAPD-INAF data processing includes modules (collected in the "CaSSIS_Reader" tool, developed in MATLAB) for the pre-processing of the raw data (previously radiometrically calibrated by the CaSSIS operations team at the University of Bern (Thomas, CaSSIS Operation paper, 2021), (Pommerol, 2021), that perform the preparation of the inputs (images and geometric parameters) for the subsequent photogrammetric processing. This tool implements the removal of the geometric distortion and the creation of the rectified mosaicked images.

The mosaicking procedure follows several steps. The exterior

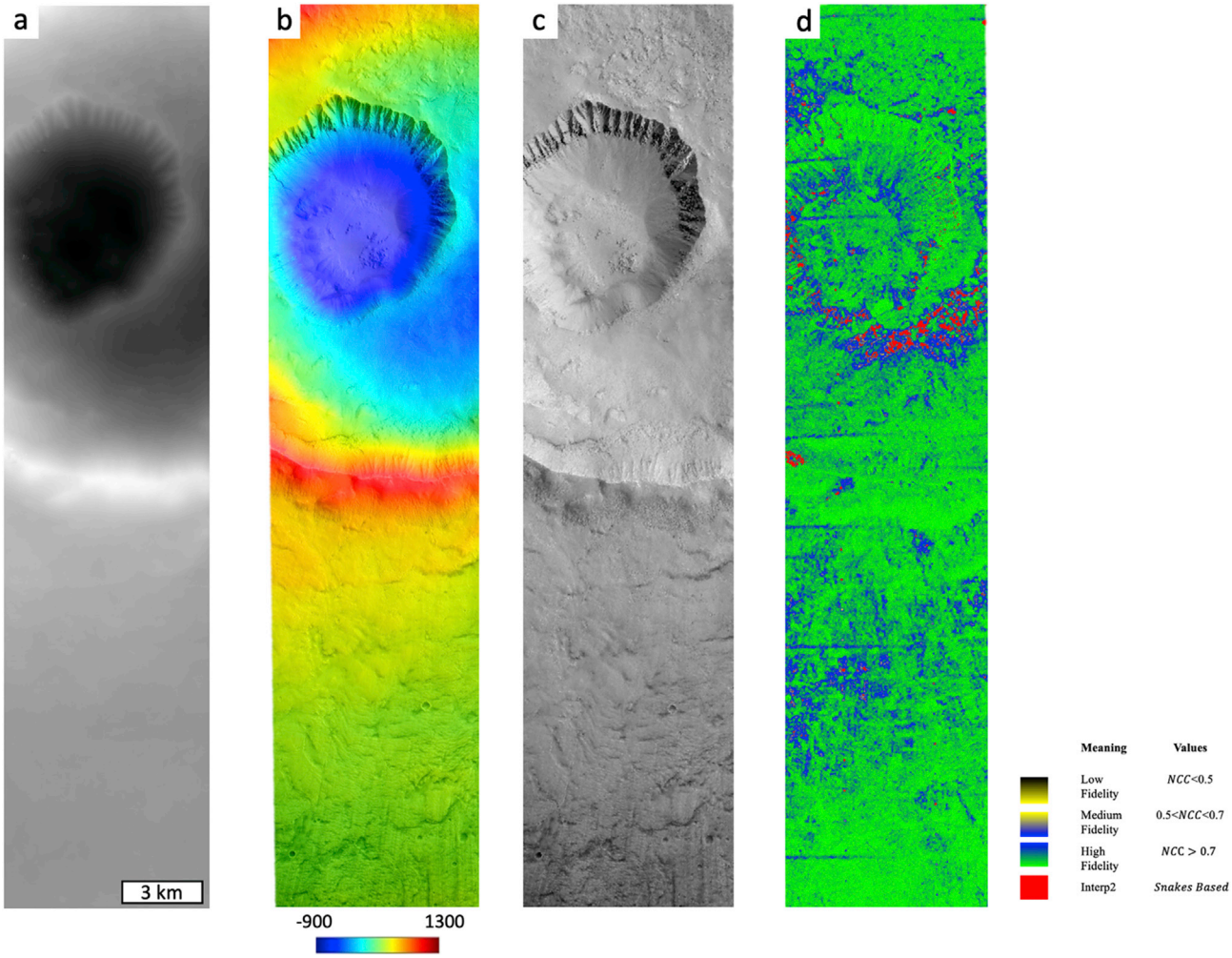

Fig. 4. a) DTM derived from the MY34_005684_218 stereo couple acquired on 2019-03-03 at 07:04 during STP (Short Term Plan) 46 with centre at 129.4334E, −35.8017N in grayscale mode, b) Coloured and texturized heightmap. Heights (in metres) reported in the colour-bar is relative to the MOLA datum (https://pds-geosciences.wustl.edu/missions/mgs/megdr.html). c) Panchromatic orthoimage, d) Figure of Merit. The stereo products can be downloaded from the Repository website: https://cassis.oapd.inaf.it/archive/cassis/showdtm.php?dtmid=119.

Table 1
Anaglyph products and filter combinations.

PNG channel →	Channel 1	Channel 2	Channel 3
Product name	Left-eye image filter	Right-eye image filters	
PAN	PAN	PAN	PAN
NPB	NIR	PAN	BLU
RGB	PAN	BLU	Synthetic Blue
RPB	RED	PAN	BLU

orientation parameters are derived from the SPICE kernels (Acton Jr, 1996) as also the interior camera parameters describing the instantaneous positions and attitude of the telescope for each framelet (Tulyakov et al., 2018). A Least Squares adjustment minimizes the misalignments between the framelets introduced by jitter effects and errors in pointing accuracy. Before the start of the matching core, a further image pre-processing is applied with as an additional radiometric correction: a Gaussian low-pass filter is applied to improve the image matching by increasing the quality of the image points and reduce the possible next mismatches. For the DTM generation, the main processing task is the pre-rectification of the mosaic using a MOLA-based DTM.

Once the mosaicked images and the associated exterior orientation parameters have been prepared, the 3DPD software that implements the image matching processing is applied. The matching core consists of finding for every point in one mosaic the corresponding point in the paired mosaic. The starting set of conjugate points is derived by the tile-based implementation of the interest operator and descriptor SURF (Bay et al., 2008). Then, an initial disparity map is created applying a Delaunay triangulation of the SURF derived points and the correlation initialization is executed with the NCC algorithm (Lewis, 1995) at the first level of the image pyramid. Consecutively, for each level of the image pyramid, the matched points are then transferred to the higher resolution level where the disparity of the additional points is predicted from the neighbourhoods with a bilinear interpolation, providing the starting location (approximate values) for the sub-pixel refinement by area-based matching (Least-Squares Matching) (Gruen, 1985) in the full resolution search image.

Once the positions and attitudes of the sensor and the geometric properties of the camera are accurately determined, the image coordinates of the high dense set of corresponding points can be converted to 3D object (i.e., surface) coordinates by means of forward ray intersection that derive a contiguous model of the surface topography. The resulting point clouds show variations in the density (due to the prospective views) and therefore are interpolated on a regular grid of height values in a map coordinate system. The 3D points are transformed into geographic Latitude/Longitude/Height coordinates and converted to

Table 2
Experimental dataset.

Name	Lat-Long [°]	i [°]	Instr.	IDs	Image pixel scale [m]	DTM grid [m]
Jovis Fossae	22.8023, 242.9626	36.123	CaSSIS	MY34_005605_157_1 MY34_005605_157_2	4.6	4.6
			HiRISE	PSP_002315_2030 PSP_002592_2030	0.25	1
Hebes Chasma	−0.7411, 283.1435	41.872	CaSSIS	MY34_005050_359_1 MY34_005050_359_2	4.6	4.6
			CTX	D15_032958_1789_XN_01S077W D16_033380_1789_XI_01S077W	5.33 6.71	12
Hale Crater	−35.7922, 323.512	32.788	CaSSIS	MY34_005640_218_1 MY34_005640_218_2	4.6	4.6
			HiRISE	ESP_030715_1440 ESP_030570_1440	0.25	1
Central Peak	−18.6569, 62.6211	24.63	CaSSIS	MY34_004219_201_1 MY34_004219_201_2	4.6	4.6
			HiRISE	ESP_021639_1610 ESP_021494_1610	0.25	1
Gasa Crater	−35.802, 129.4334	38.94	CaSSIS	MY34_005684_218_1 MY34_005684_218_2	4.6	4.6
			HiRISE	ESP_021584_1440 ESP_022217_1440	0.25	1

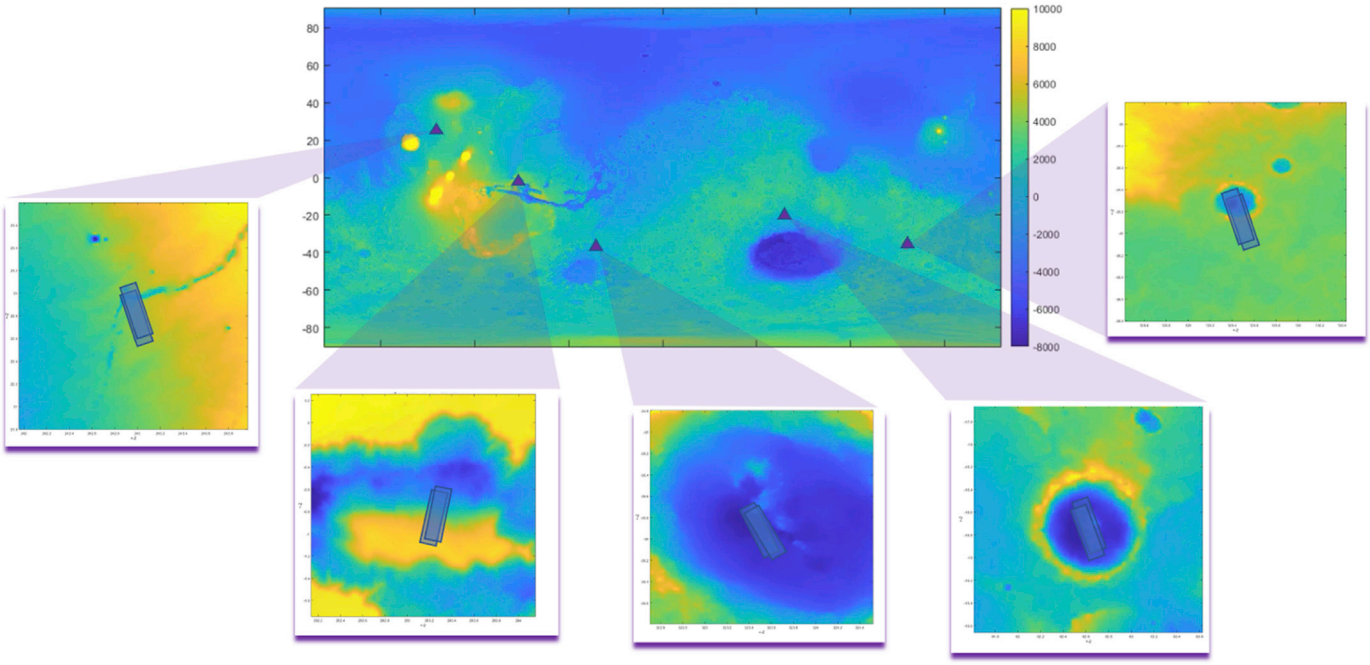

Fig. 5. Locations of the investigated regions on MOLA global DTM (the elevation colourbar is in m with respect to mean radius). From the left side to the right: Jovis Fossae, Hebes Chasma, Hale Crater, Central Peak and the Gasa Crater.

line/sample coordinates in map space using the desired map projection (Equirectangular or Polar Stereographic).

3. CaSSIS stereo products

The OAPD-INAF team has produced 263 DTMs so far on a total of more than 1700 stereo pairs acquired by the instrument (through September 2020). The locations of the targets acquired and the corresponding DTMs delivered are reported in Fig. 2 and Fig. 3, respectively.

The repository includes the DTMs that are 32-bit signed, produced in Equirectangular projection equally sampled in planetographic Latitude, with elevations referenced to the MOLA datum (version megR_hb - https://pds-geosciences.wustl.edu/missions/mgs/megdr.html). The DTM spatial resolution is strictly related to the image quality and to the accuracy of the orientation data so the grid spacing depends on the acquisition conditions. For the time being, a nominal stereo pair acquired at 4.6 m/pix provides a DTM with 15 m/pix post sampling as for the case presented in (Simioni et al., 2021). The 3DPD software also permits the generation of DTMs "at every pixel" (on a grid with post spacing equal to the image resolution: 4.6 m/pix).

The outputs of the 3DPD pipeline include also orthoimages (Fig. 4-c) for all the filters (either in I/F reflectance or raw signal in DN – digital numbers). Additional products are provided for a better exploitation and visualization of the DTM, such as a colour height map (Fig. 4-b) and the "Figure of Merit" (Fig. 4-d) for the definition of the quality of the matching for each pixel of the gridded DTM.

4. Anaglyph processing

Another CaSSIS stereo product is represented by Anaglyphs, produced by the University of Arizona team. These products, which can be viewed in 3D with standard red-blue glasses, are assembled by placing the image

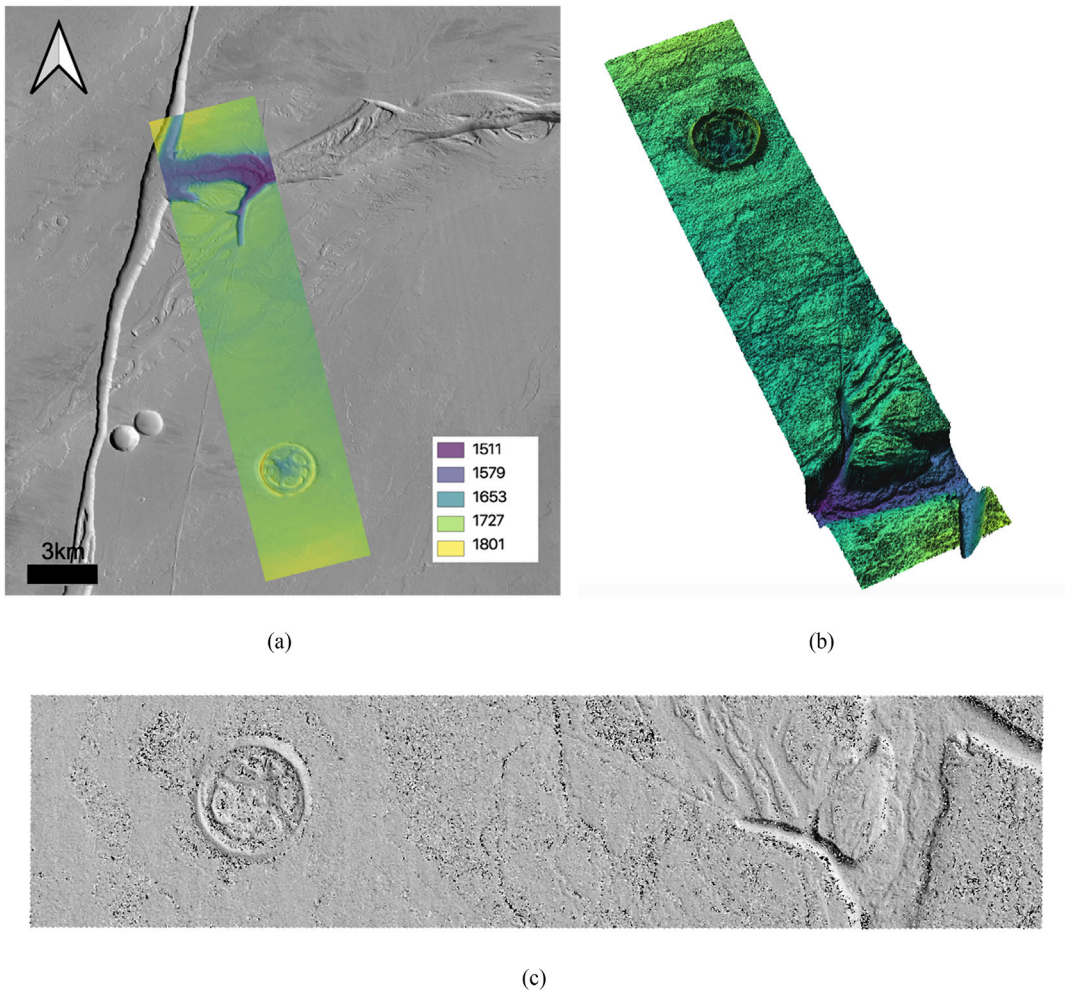

Fig. 6. Jovis Fossae DTM generated from CaSSIS images MY34_005605_157_1 and MY34_005605_157_2. (a) The height map superimposed on a CTX basemap (http://murray-lab.caltech.edu/CTX). (b) The 3D visualization. (c) The hillshade DTM.

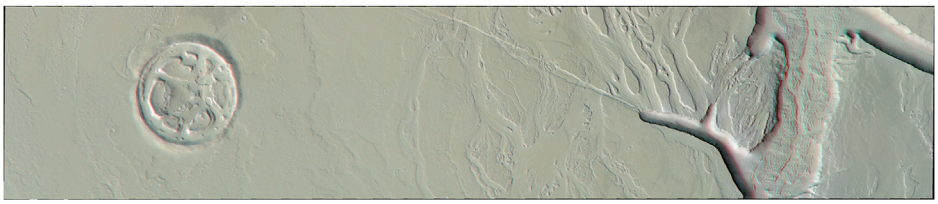

Fig. 7. Stereo anaglyph of the Jovis Fossae region produced from the CaSSIS stereo pair MY34_005605_157 (Product: MY34_005605_157 _NPB.anaglyph.png). The topography can be visualised using standard blue/red stereo glasses.

from one half of a stereo pair into the red channel (for the left eye) and the image from the other half of the stereo pair in the green and blue channels (for the right eye) of an RGB image. Anaglyphs can aid in the qualitative analysis of complex surfaces with a minimized amount of computational and personnel resources. They also make exceptional products for public outreach. The automated pipeline has produced analyphs for over 1000 stereo pairs. Processing of newly acquired stereo pairs continues, while backfilling anaglyphs for stereo pairs acquired prior to the completion of the automated pipeline is ongoing.

The CaSSIS anaglyph pipeline uses a similar method to that implemented to produce HiRISE anaglyphs (McEwen et al., 2010). A stereographic projection is used, making the along-orbit pixel scales across the images equal. This is done to make co-registering the two images possible. The MOLA DTM is not used for projecting the images used in making anaglyphs. We do not want to correct for topographical effects, as is the case in orthoimages. We want to retain the terrain distortions, because that is the information anaglyphs are intended to reveal. Instead, the mean radius over the intersection of the two images is extracted from the MOLA DTM. Each image is then mapped onto a spherical shape model with this mean radius. The angle of separation for CaSSIS stereo images is in the along-track direction, thus the parallax is in the along-track direction. Human eyes are spaced horizontally, so the images that make up the CaSSIS anaglyphs, nominally directed with along-track direction parallel to meridians, must be rotated so that the parallax is in the direction that matches our eyes. This results in the horizontal edges in non-projected images becoming the vertical edges in the anaglyph products.

The automated processing pipeline is written in Python and makes extensive use of US Geological Survey's (USGS) Integrated Software for Imaging Spectrometers (ISIS) (Becker et al., 2018). The anaglyph

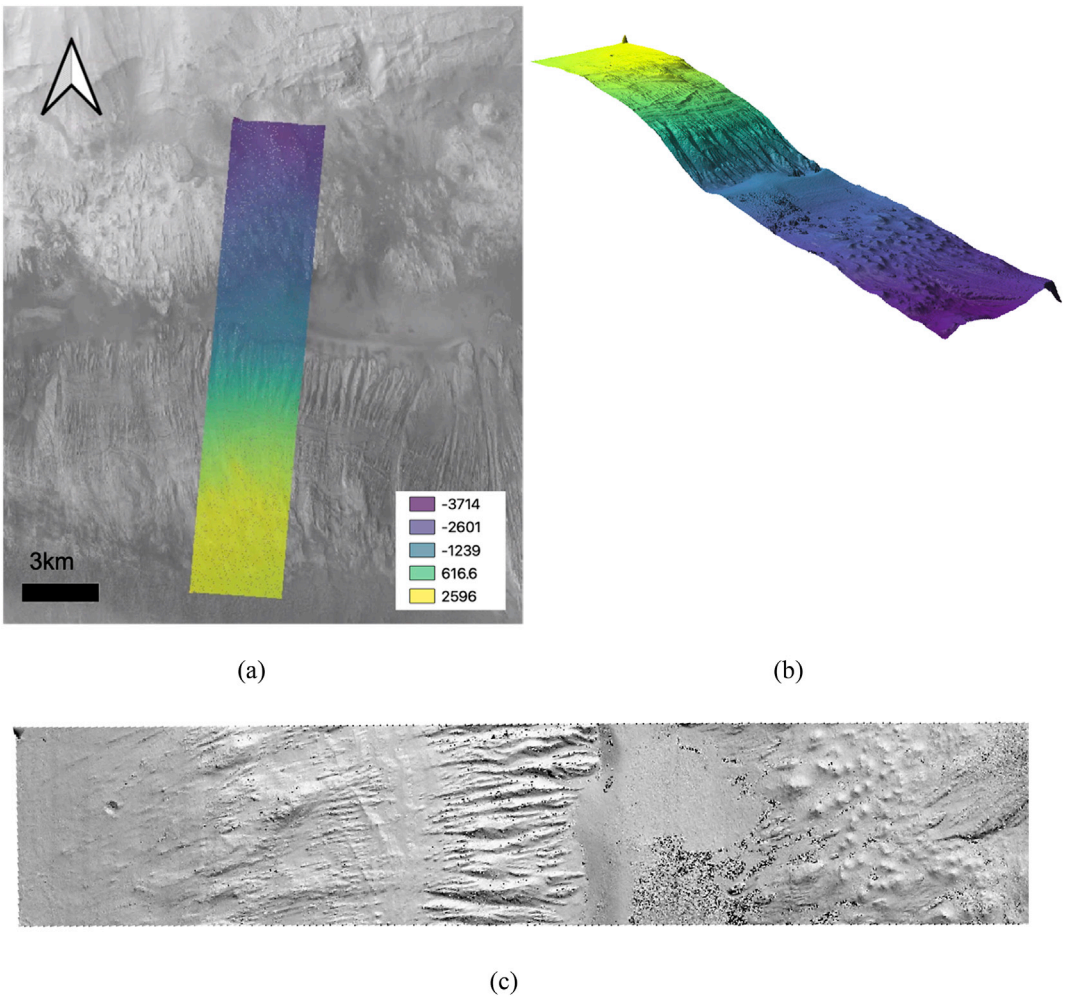

Fig. 8. *Hebes Chasma DTM generated from CaSSIS images MY34_005050_359_1 and MY34_005050_359_2. (a) The height map superimposed on CTX basemap (*http://murray-lab.caltech.edu/CTX*) . (b) The 3D visualization. (c)The hillshade DTM.*

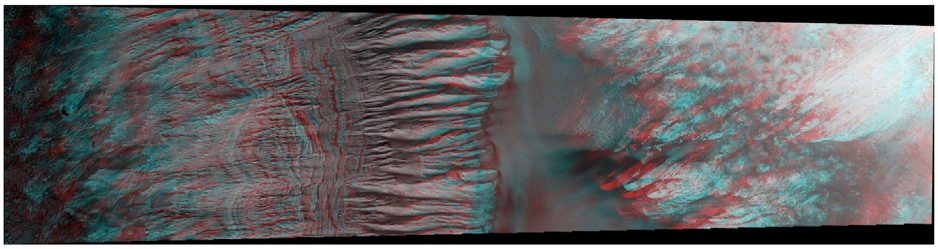

Fig. 9. Stereo anaglyph of the Hebes Chasma region produced from the CaSSIS stereo pair MY34_005050_359 (Product: MY34_005050_359_PAN.anaglyph.png). The topography can be visualised using standard blue/red stereo glasses.

processing pipeline starts with radiometrically corrected framelets and consists of the following steps that are described in subsequent sections:

1. Map projection and mosaicking of images (§4.1)
2. Co-registration of images (§4.2)
3. Assembling anaglyph products (§4.3)

4.1. Map projection and mosaicking

Each CaSSIS framelet is imported into an ISIS-formatted cube. Initially, standard SPICE information is attached to each framelet so that the observation geometry can be obtained for both images. This observation geometry is used to find the mean planetary radius over the intersection of the two images and a custom Planetary Constants Kernel (PCK) is created by replacing all 3 body radii with this mean radius. The custom PCK is then applied to each framelet. The geometric and photometric information is computed at the center of each image. This information is used to calculate the map projection rotation required for optimum parallax. Each framelet is then map projected and the framelets from each image are mosaiced together for each filter.

4.2. Co-registration

Uncertainties in spacecraft pointing and attitude, rotation mechanism and jitter can cause misregistration between the two images. The two

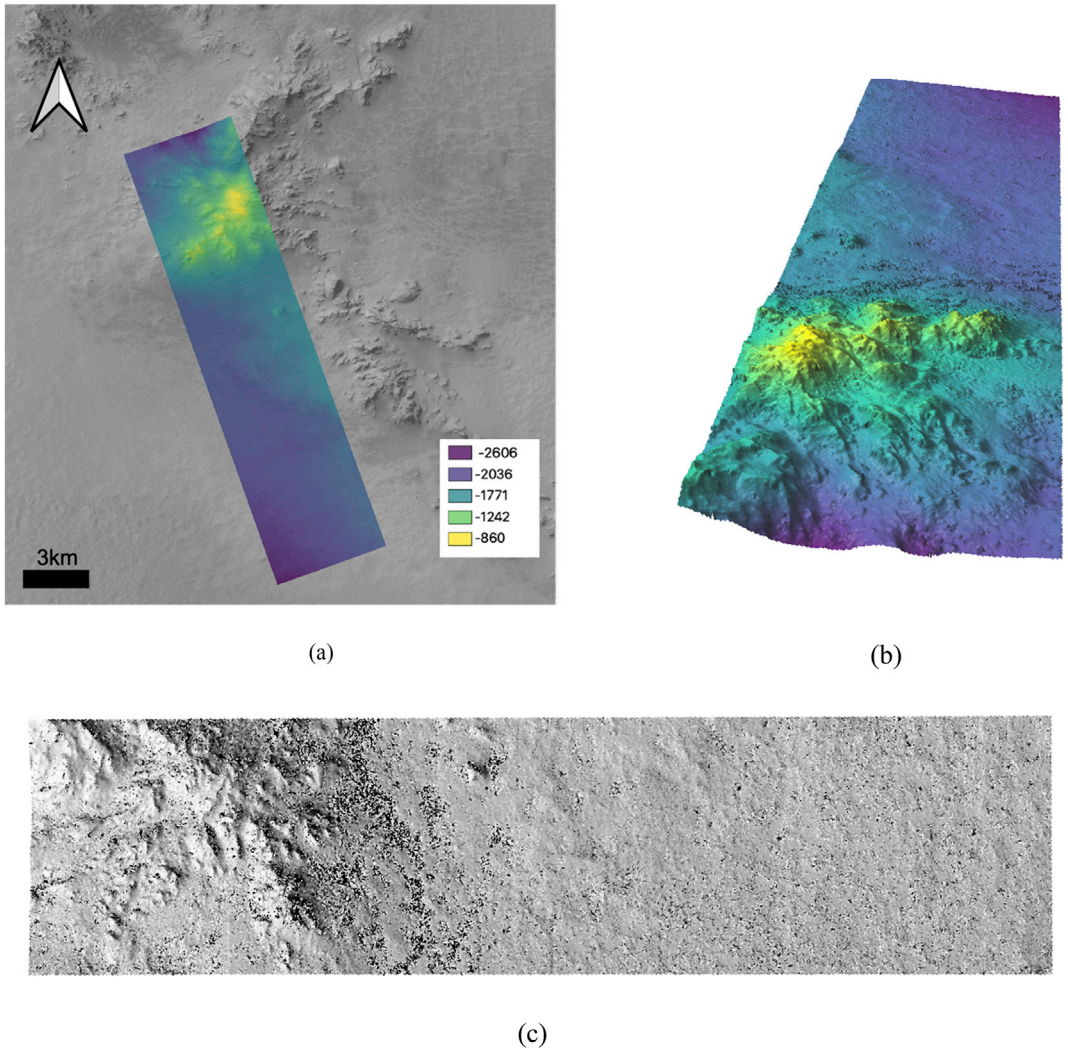

Fig. 10. Hale Crater DTM generated from CaSSIS images MY34_005640_218_1 and MY34_005640_218_2. (a) The height map overlapped on CTX basemap (http://murray-lab.caltech.edu/CTX). (b) The 3D visualization. (c)The hillshade DTM.

Fig. 11. Stereo anaglyph of the Hale Crater region produced from the CaSSIS stereo pair MY34_005640_218 (Product: MY34_005640_218_NPB.anaglyph.png). The topography can be visualised using standard blue/red stereo glasses.

images need to be co-registered prior to assembling the anaglyph. A rigid transformation is performed on one half of the stereo pair, with respect to the other half, to get proper vertical alignment and parallax between the two images. There are two key challenges to automating anaglyph processing without operator intervention. The first challenge is achieving good vertical alignment between surface features across the two images. It is crucial that there is very little vertical misalignment of surface features. This type of misalignment makes the anaglyph uncomfortable for the viewer to look at and degrades the stereo quality. The second challenge is maintaining optimum horizontal separation, which creates the 3D effect. Separation in the horizontal direction is inherent and required for 3-D viewing, but it is important for the comfort of the viewer that this separation not be too large. The pattern matching algorithm used in our pipeline is maximum correlation with a defined tolerance for goodness of fit. Co-registering the two images can be an iterative process. We begin by using a default point grid density and tolerance. The quality of the co-registration is gauged by a sufficient number of matched points and a low standard deviation for the line translation. For quality images with good a signal to noise ratio (SNR), these default parameters are usually sufficient. However, low SNR, smooth surfaces, or haze in an image can degrade the quality of the co-registration. If an insufficient number of matched points is found, the point grid density will be increased. If the line standard deviation is more than a few pixels, the tolerance is iteratively increased to exclude suspect matches, until an acceptable line

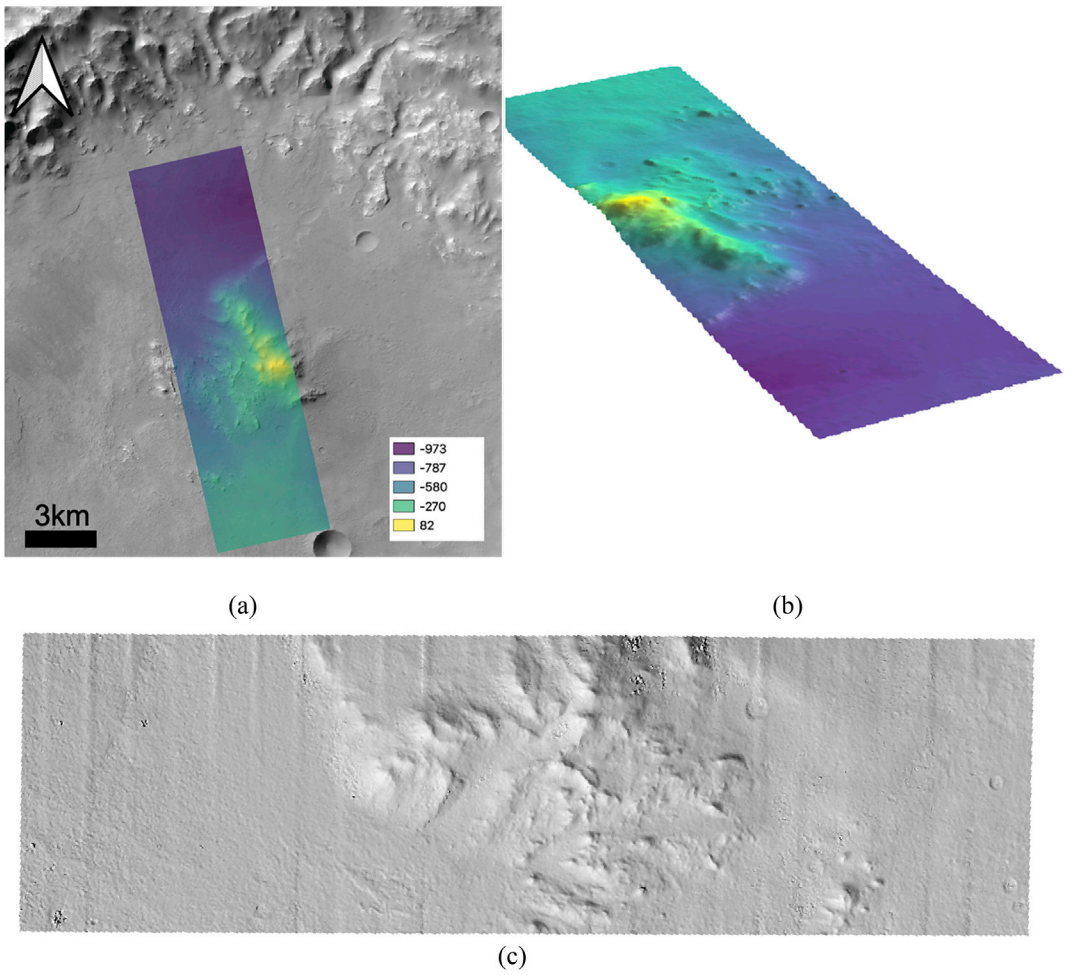

Fig. 12. Central Peak DTM generated from CaSSIS images MY34_004219_201_1 and MY34_004219_201_2. In (a) the height map overlapped on CTX basemap (http://murray-lab.caltech.edu/CTX). (b) The 3D visualization. (c)The hillshade DTM.

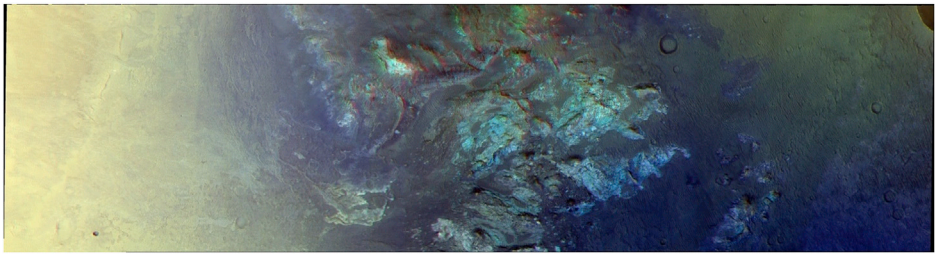

Fig. 13. Stereo anaglyph of the Central Peak region produced from the CaSSIS stereo pair MY34_004219_201 (Product: MY34_004219_NPB.anaglyph.png). The topography can be visualised using standard blue/red stereo glasses.

standard deviation is achieved. The smaller the line standard deviation, the better the vertical alignment between the two images. The parallax is expressed in the sample direction, therefore a larger standard deviation in sample matched points is expected. It was found that using average sample translation resulted in comfortable horizontal separation. By employing the above process, the co-registration step can be fully automated.

4.3. Assembling

The appropriate halves of the stereo pair and filters are then assembled into the final anaglyph products. These products are standard 8-bit RGB PNGs. Both gray-scale and colour anaglyphs are currently being produced through this automated processing. Monochromatic (gray-scale) anaglyphs are created by using the same filter for all three channels of the PNG, while using different filter combinations in the three channels creates various colour anaglyphs. The panchromatic (PAN) filters from each half of a stereo pair are used to create gray-scale anaglyphs. Colour anaglyphs are created by using the PAN filter with different combinations of the three broadband filters (NIR, RED, BLU). In this way, PAN, NPB, simulated RGB and RPB colour anaglyphs can be created as illustrated in Table 1. Simulated RGB products are created using the PAN image in channel 1, the BLU image in channel 2 and a “synthetic blue” image in channel 3. The synthetic blue image is created by multiplying

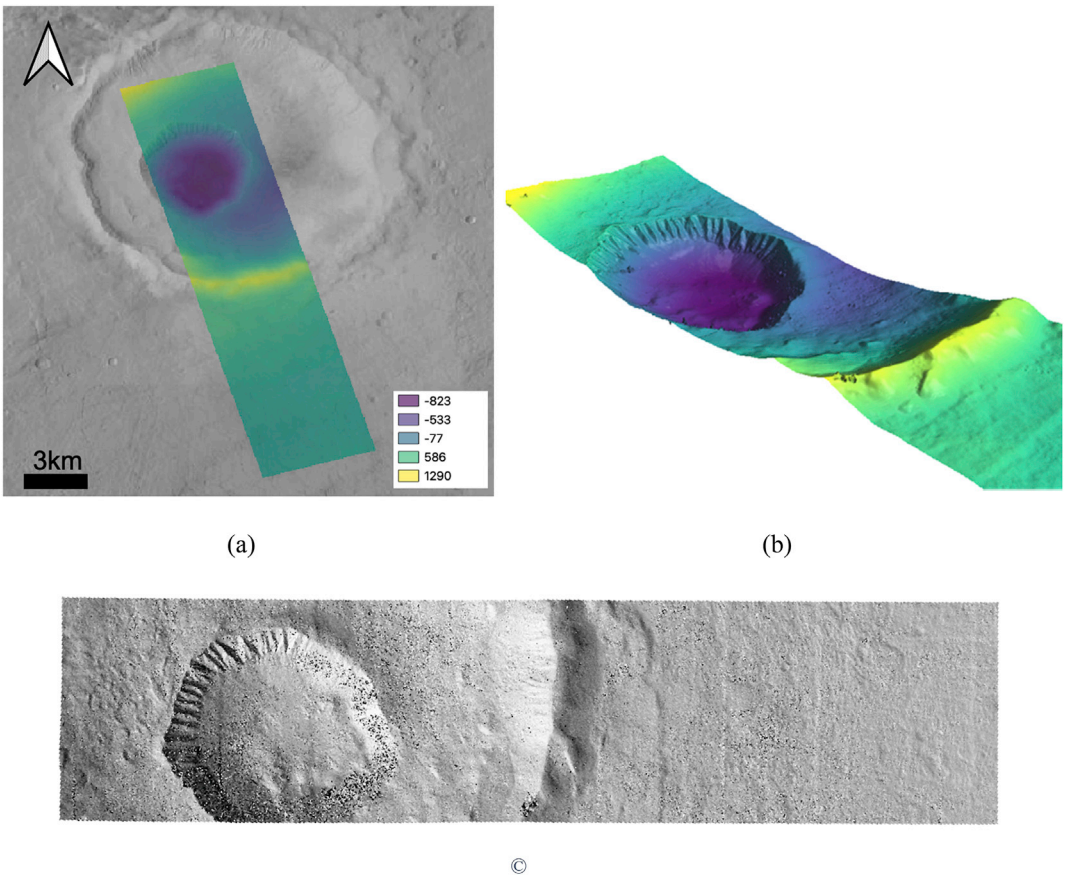

Fig. 14. Gasa crater DTM generated from CaSSIS images MY34_005684_218_1 and MY34_005684_218_2. (a) The height map superimposed on CTX basemap (http://murray-lab.caltech.edu/CTX). (b) The 3D visualization. (c)The hillshade DTM.

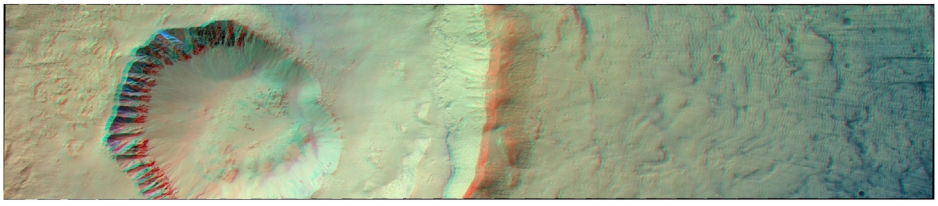

Fig. 15. Stereo anaglyph of the Gasa Crater region produced from the CaSSIS stereo pair MY34_005684_218 (Product MY34_005684_218_NPB.anaglyph.png). The topography can be visualised using standard blue/red stereo glasses.

Table 3
Number of seed points and Statistics of the Local Signal Standard Deviation (mean and STD).

Test	Seed points	Mean	STD
Jovis Fossae	1206	0.2624	0.2496
Hebes Chasma	3313	0.3662	0.2514
Hale	1526	0.2402	0.2324
Central Peak	3752	0.3491	0.2447
Gasa Crater	1678	0.2922	0.2422

the BLU image by 2 and subtracting 30% of the PAN image. This emulates the method HiRISE uses to create their RGB colour "extras" products (Delamere et al., 2010).

5. Methodology and experimental data

The relative quality of the output DTM largely depends on the dense matching algorithms applied, which are dependent on the quality of the images themselves both in terms of radiometric content (Pommerol, 2021) and geometric properties (Tulyakov et al., 2018); while the issues concerning absolute accuracy are not considered in this context. Since the quality of the DTMs affects the accuracy in computing multiple morphometric indexes (i.e., mean gradients, sharpness, curvature maps and slope maps) directly extracted from the 3D topographic models, the importance of producing highly accurate and precise DTMs become mandatory and their assessment of great interest. The tests include varying the photogrammetric processing parameters, and then extrapolating correlations between those settings and the image quality or the morphological characteristics. The best approach to evaluate the quality of the DTMs under investigation is to use a reference dataset with higher precision, possibly with higher resolution and dense sampling and broad spatial coverage (Kirk et al., 2020). In order to perform good comparison with the reference dataset, the reference and test DTMs need to be co-registered.

With these considerations, the comparisons have been performed using the DTMs produced stereogrammetrically with HiRISE (McEwen et al., 2007) (Kirk et al., 2008), which provide the highest resolution

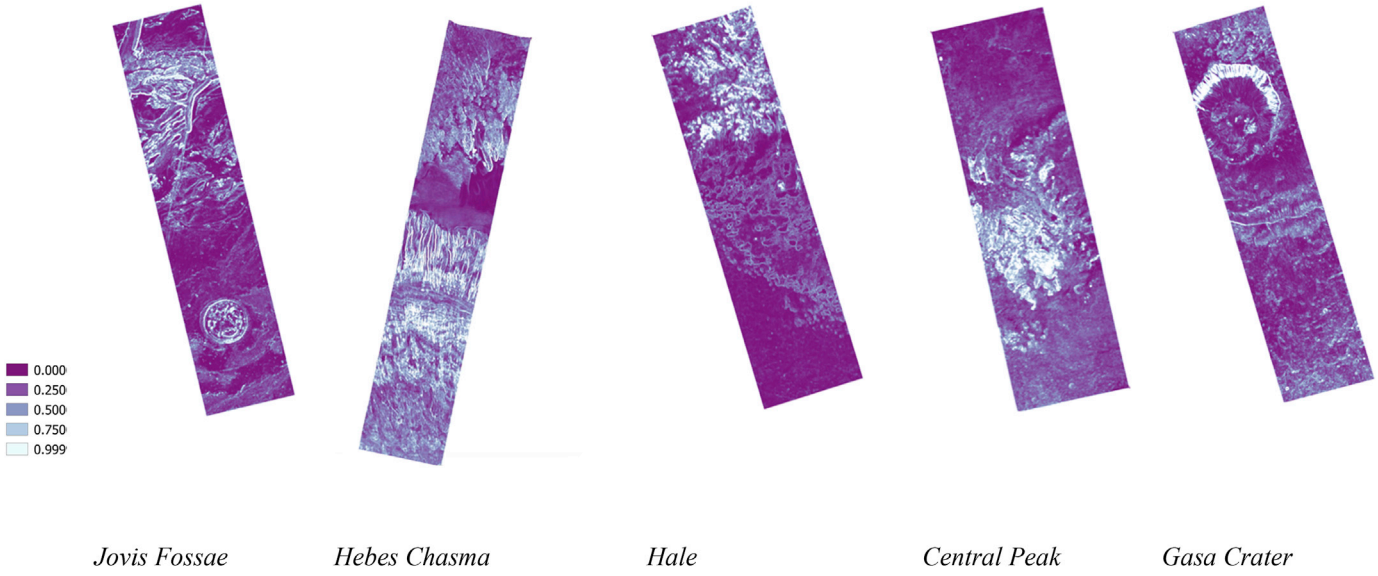

Fig. 16. From the Left to the Right the coloured maps of the normalized local signal Standard Deviation obtained with a kernel of 23x23 pixels.

images in the Mars context (25 cm/pixel), and with the 6 m/pixel images of CTX (Malin et al., 2007). Comparison with DTMs generated from CTX fortuitous stereoscopic coverage have also been performed. With 119, 000 images today at ~6 m/pixel, CTX imagery covers most of the planet between 85°N and 85°S with frequent overlap, providing means to evaluate the quality of CaSSIS DTMs with DTMs generated from another dataset of similar resolution.

5.1. Dataset

Five different regions have been examined as experimental dataset (Table 2) for the CaSSIS DTM production applying the photogrammetric processing procedures proposed by OAPD-INAF and for the anaglyphs generation.

The areas span over a range of latitudes between 50°N and 40°S covering different terrain morphologies. Furthermore, the illumination conditions (in terms of solar incidence angle) vary between ~ 30° and ~ 60°.

The dataset considered includes:

- Jovis Fossae: Volcanic terrain with channels
- Hebes Chasma: Layered deposits
- Hale Crater: Etched terrain
- Central Peak: Etched terrain
- Gasa Crater: Crater rim terrain

Detailed descriptions of each area and the scientific context are provided in following sections.

The regions were selected by meeting the stereo coverage requirement with CaSSIS in stereo mode and also having HiRISE DTMs available. CTX stereo products are also present over one area of interest in order to dispose of the DTMs needed for the comparisons.

The supporting (reference) DTMs derived from HiRISE have been produced by the University of Arizona and retrieved from the HiRISE website (http://hirise.lpl.arizona.edu). The PDS HiRISE DTMs for each region (previously enlisted) are the following respectively:

DTEEC_002315_2030_002592_2030_A0, DTEEC_030715_1440_030570_1440_A01, DTEEC_008823_2310_009245_2310_A01 and DTEED_014081_1440_014147_1440_A0.

The SOftCopy Exploitation Tool Set, called BAE SOCET® Set (SS) (Miller and Walker, 1993) applying the NGATE strategy (Zhang et al., 2007) has been used for creating DTMs using the methods described in (Kirk R. L., et al., 2008).

USGS-ISIS (Becker et al., 2018) is used to reformat the level-0 input into level-1 radiometrically corrected images which are then ingested into SS for bundle adjustment and stereo matching as well as grid-point interpolated onto a regular DTM as described by (Kirk et al., 2008).

The CTX DTM (covering Habes Chasma) has been generated using the NASA Ames Stereo Pipeline (https://ti.arc.nasa.gov/tech/asr/groups/intelligent-robotics/ngt/stereo/) (Beyer et al., 2018) as implemented in the MarsSI application (https://marssi.univ-lyon1.fr/MarsSI/).

Table 2 reports the IDs of the CaSSIS and HiRISE stereo pairs, image and DTM resolution, illumination conditions for CaSSIS acquisitions and the centre location. A visualization of the distribution of these DTMs on the equirectangular MOLA map is shown in Fig. 5.

5.1.1. Jovis Fossae

The "Jovis Fossae" region (22.8023°N, 242.9626°E) has been covered by CaSSIS with the stereo pair MY34_005605_157 (Fig. 6-Fig. 7). The stereo coverage captures the junction of the terminus of the 420-km long Olympica Fossae with Jovis Fossae in the northeastern section of the Tharsis Volcanic Province. A complex channel system of possible volcanic or fluvial origin (Mouginis-Mark, 1990) (Plescia, 2013) exists within and around Olympica Fossae. The regional geologic context is the Late Hesperian–Amazonian volcanic plains south of Alba Mons, and to the east of Olympus Mons (Tanaka et al., 2014). Where the two fossae meet, Jovis is 60–80 m deep and 1–2 km wide (Supplementary Fig. 1). Olympica is 2–4 km wide and is 200–300 m deep. The floor of Olympica is covered by rough textured flows with a central incised channel. Surface textures of the floor-covering flow display pressure ridges, indicating a volcanic flow morphology (Plescia, 2013). The depth of the central incised channel is up to 53 m, placing a lower limit on the flow thickness on the floor of the channel itself. Accurate topographic analysis of this region is critical to understanding the interaction of tectonic, volcanic, and hydrological processes.

5.1.2. Hebes Chasma

The "Hebes Chasma" region (0.7411°S, 283.1435°E) has been covered by CaSSIS with the stereo pair MY34_005050_359. This area shows two levels of hydrated sulfate units of the Valles Marineris Interior Layered Deposits (ILD) identified by (Schmidt et al., 2018). The main ILD unit, on the central mound of Hebes Chasma, corresponds to yellow and green colours on Fig. 8, and the left side of Fig. 9. ILDs located on the mound are a good test for topography, owing to the difference in layer

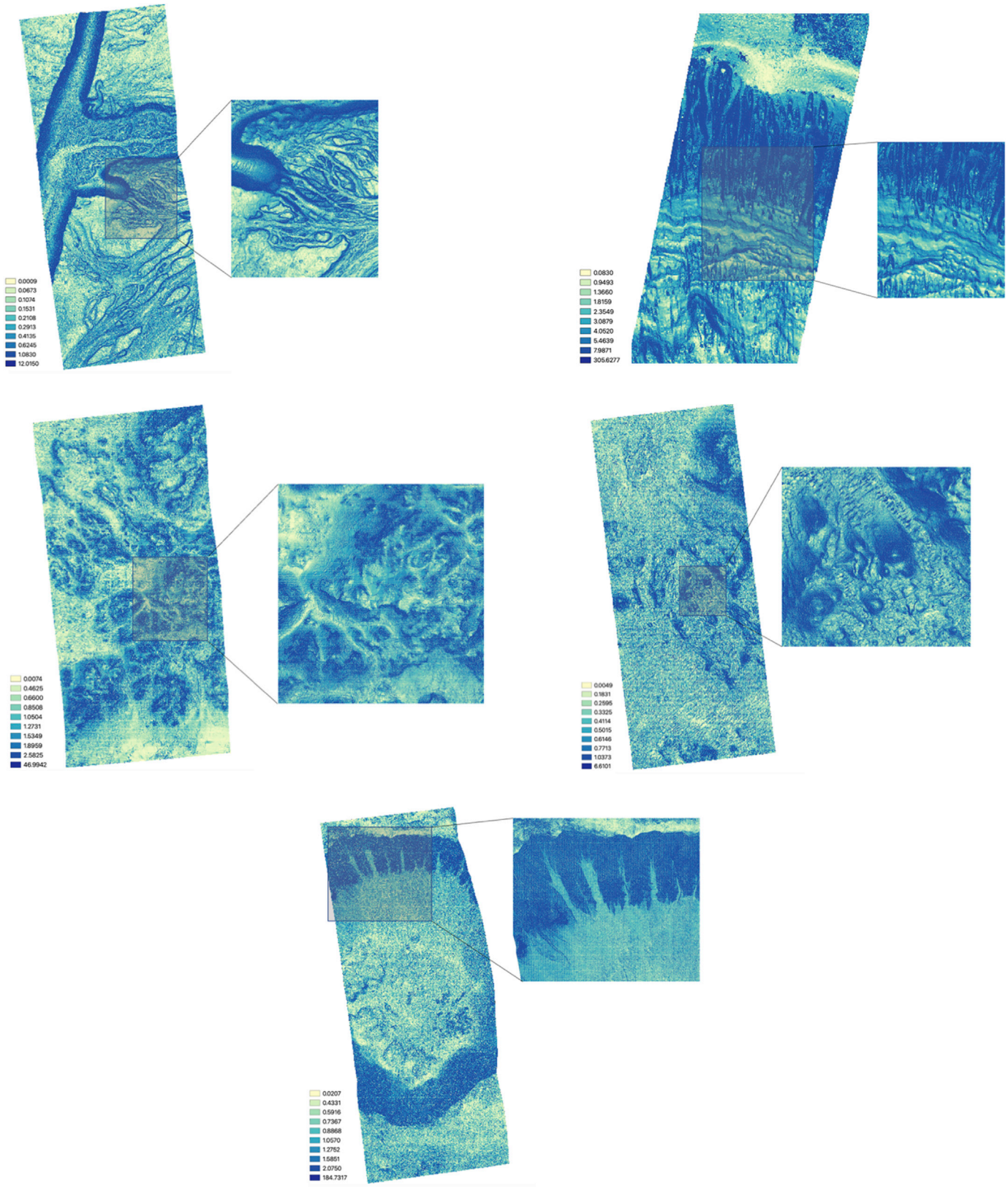

Fig. 17. Colour Maps of the surface roughness with closeup views. From the top left: Jovis Fossae, Hebes Chasma, Hale, Central Peak and Gasa.

strength, which results in topographic scarps. The CaSSIS DTM makes it possible to quantify the height of the scarps between 2 m and several tens of meters. Other scarps, interpreted as resulting from ILD fracturing, are also well apparent on the contour map (Supplementary Fig. 2). The other ILD unit, in violet on Fig. 8 and at the left edge of Fig. 9, is eroded forming yardangs, the topography of which can be followed, giving a height of 10–20 m.

Table 4
Standard Deviation of the Roughness values for each region.

Test	STD Roughness
Jovis Fossae	0.614
Hebes Chasma	6.630
Hale	1.190
Central Peak	0.399
Gasa Crater	1.180

Table 5
Expected Vertical Precision (from theoretical formula, Eq. (4)).

Test	EP (m)
Jovis Fossae	4.9602
Hebes Chasma	4.8342
Hale	4.6488
Central Peak	5.0703
Gasa Crater	4.8552

Table 6
STD Values of the discrepancies over the whole overlapping areas visualised in Fig. 18.

Test	STD (m)	Mean (m)
Jovis Fossae	8.03	0.58
Hale	38.55	7.99
Central Peak	10.68	1.27
Gasa Crater	19.31	−2.73

5.1.3. Hale Crater

The "Hale Crater" region (35.7922°S, 323.5119°E) has been covered by CaSSIS with the stereo pair (MY34_005640_218) (Fig. 10-Fig. 11). One of Hale's geologic interest is its very active surface processes (Kolb et al., 2010) (Munaretto et al., 2020). In particular, the central peak displays intense Recurring Slope Linae (RSL) activity (McEwen et al., 2011), with some parameters, such as RSL length, which depend on the slope angle (Munaretto et al., 2020). Although this conclusion was drawn from a HiRISE DTM analysis, similar studies can now be performed on the CaSSIS DTM (Supplementary Fig. 3), where slope variations are found parallel to the slope variations measured on the HiRISE DTM. When there is a need for broader coverage, such as in this setting, CaSSIS DTMs can be used instead of HiRISE DTMs.

5.1.4. Central peak

The "Central Peak" (18.6569 °S, 62.6211°E) of a crater ~50 km across, and located southeast of the Huygens crater has been covered by CaSSIS with the stereo pair (MY34_004219_201) (Fig. 12-Fig. 13). The peak shows an exceptionally huge exposure of fractured bedrock uplifted by the impact over a section of 800 m vertically (Supplementary Fig. 4). Light bedrock outliers alternate with darker dune deposits, and highlight the difference in slope angle between the deposits and bedrock. The slope angle of the deposits is generally <5°, frequently much less. Bedrock exposure has uneven topography with smooth, fractured monoclinal slopes up to 11°, and mounds with slope angles up to 25°. In the absence of major fracturing between the smooth bedrock slopes and the mounds, the geologic difference between mounds and gentler bedrock slopes is likely due to local differences in rock strength.

5.1.5. Gasa Crater

Gasa crater (35.8017°S, 129.4334°E) has been covered by CaSSIS with the stereo pair (MY34_005684_218) (**Error! Reference source not found.**-Fig. 15). The crater is a very fresh impact crater, dated at less than 2.1 Ma (Schon, 2012) with a sharp rim-crest and well-defined flat floor and is located within an older crater in eastern Promethei Terra. The crater displays glacial landforms dating back to the most recent period of higher obliquity (Schon, 2012) and many gullies originating from alcoves rooted at the top of the crater. The structure and morphology of the alcoves were used to model the conditions of gully development (Okubo et al., 2011). The CaSSIS DTM makes possible to quantify the crater morphology quantitatively, showing for instance that the slopes of the spur crest lines, up to ~30°, gradually lowering toward the bottom of the crater to values down to ~15°, with a very fast transition between 15° and the flat floor (Supplementary Fig. 5). The precision of the CaSSIS DTM enables the investigation of the conditions of gully development, between the spurs and the crater floor, as well as the details of the spur morphology from which H_2O was removed, leading to the gully genesis.

5.2. Image quality analysis

Photogrammetric processing algorithms generally suffer from problems related to the initial image quality and intrinsic characteristics (noise, shadows, texture-less regions, low radiometric quality, etc.) resulting in noisy 3D points or issues in extracting features. Therefore, the quality of the image matching can be directly affected by poor image quality. A statistical analysis of the stereo pairs has been performed in terms of normalized local signal Standard Deviation (σ) (mark of the local contrast). This local analysis has been conducted to obtain the distribution of the image contrast with the purpose of checking possible correlation between this image quality index and the final 3D product.

The image contrast can be controlled by the illumination conditions also in relation with the surface curvature and slope as well as determined from the intrinsic surface variegations of course.

Since the area-based matching algorithms work with small sub image areas, a local signal analysis appears more appropriate than the global one (Gwinner et al., 2009). Furthermore, the contrast seems to be helpful to produce high number of tie points extracted to be used as seed points (first approximated disparity map) in the dense matching process as reported in Table 3 for each region analyzed. It is important to remark that the number of seed points depends on the dimension of the CaSSIS images, which varies from one image to another.

In Table 3 are also reported the statistics relative to the Normalized Local Standard Deviations (within 2 Sigma) extracted from the master images of each region considered and in Fig. 16 the corresponding colour coded maps.

What emerges, looking at the colour maps and confirmed by the statistics of the local signal STD, is that the "Central Peak" and the "Hebes Chasma" regions are the areas where the local contrasts are higher and largely distributed across the terrain.

5.3. Processing parameters and terrain analysis

The regions described above have been considered to assess the capabilities of CaSSIS for the generation of high resolution DTMs. These areas of high scientific interest, and with different morphological characteristics and terrain roughness, provide the opportunity to test, in particular, the capability of the stereo products to support the interpretation of specific features.

In the 3DPD pipeline, several options and parameters can be changed to control the processing.

The performance of the matching processing, in particular, can be strongly affected by different contingencies such as: the low amount or complete lack of texture and contrast, poor SNR or radiometric artifacts. Surface properties also play a significant role, such as curvatures and discontinuities, occlusions, shadows, etc.

The main tunable matching parameters in our procedure are the matching window (template) size and the shape model implemented in the Least Square matching (LSM) algorithm. Different types of transformations (shape models) can be applied to the matching window of the patch image to minimize the difference from the template (window

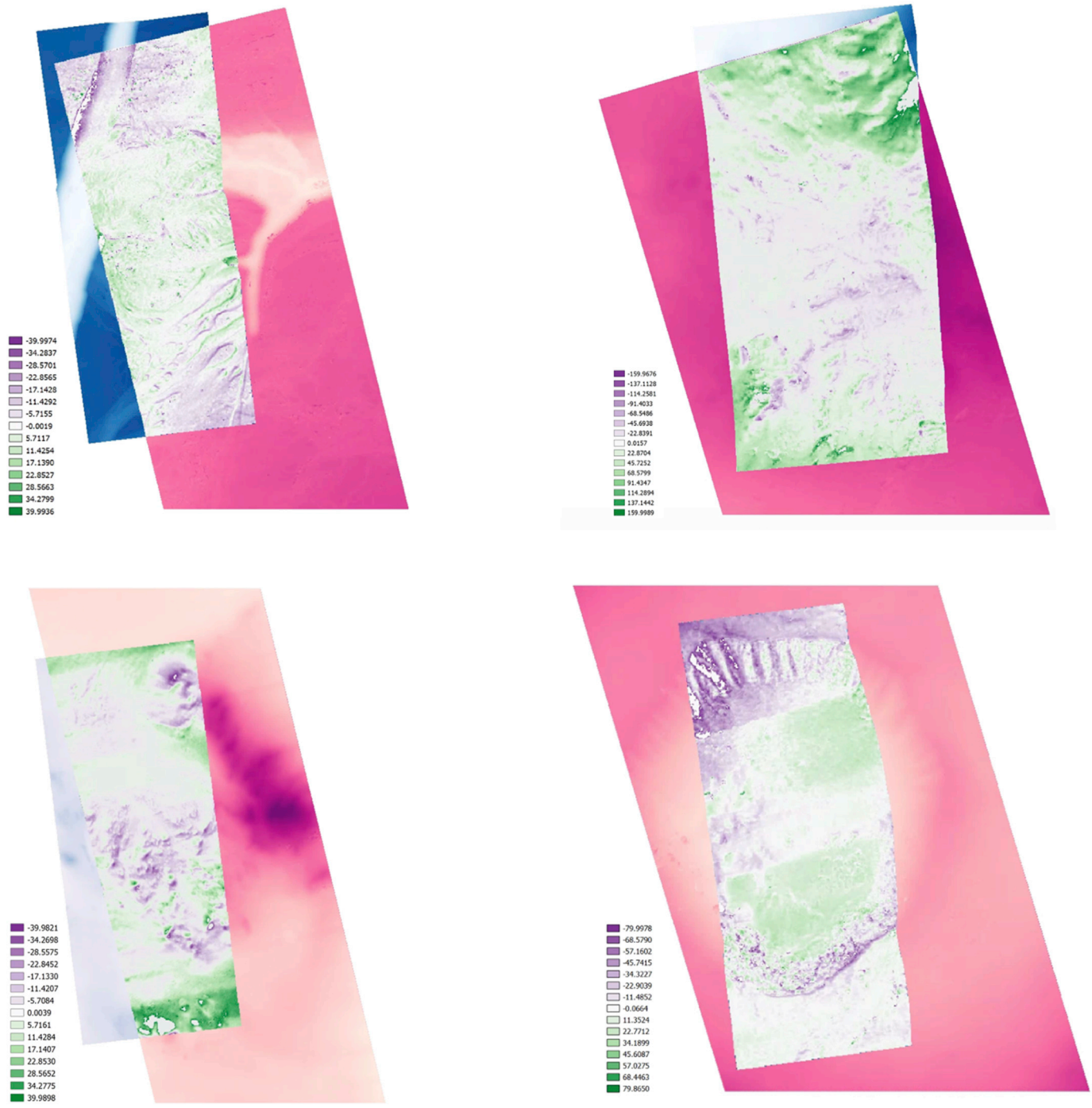

Fig. 18. For each region (from top left, to bottom right: Jovis Fossae, Hale, Central Peak and Gasa): CaSSIS DTM in pink shaded version, HiRISE DTM in blue shaded version and in the overlapping region the colour coded version of the discrepancies. The colour scale bars are given in meters and the limits are correspondent to four times the overall STD.

extracted on the master image).

An affine transformation (6-parameters transformation as reported in Equation (1)) is used as the default geometric transformation but our implementation also provides alternative functional models for the geometrical transformation involved in the LSM to handle perspective differences.

In particular, the projective transformation (8-parameters transformation Eq. (2)), which implements a homography model, aims specifically at convergent image pairs while the n-order polynomial model (12-parameters transformation, Eq. (3)), is meant to improve the modelling when the surface consists of curvatures within the matching patch.

The following equations describe the three transformations mapping the x, y original coordinates of the patch template to the transformed u, v.

$$u(x,y) = a_0 + a_1x + a_2y\,; \quad v(x,y) = b_0 + b_1x + b_2y \qquad \text{(Equation 1)}$$

$$u(x,y) = \frac{a_0 + a_1x + a_2y}{1 + c_1x + c_2y}; \quad v(x,y) = \frac{b_0 + b_1x + b_2y}{1 + c_1x + c_2y} \qquad \text{(Equation 2)}$$

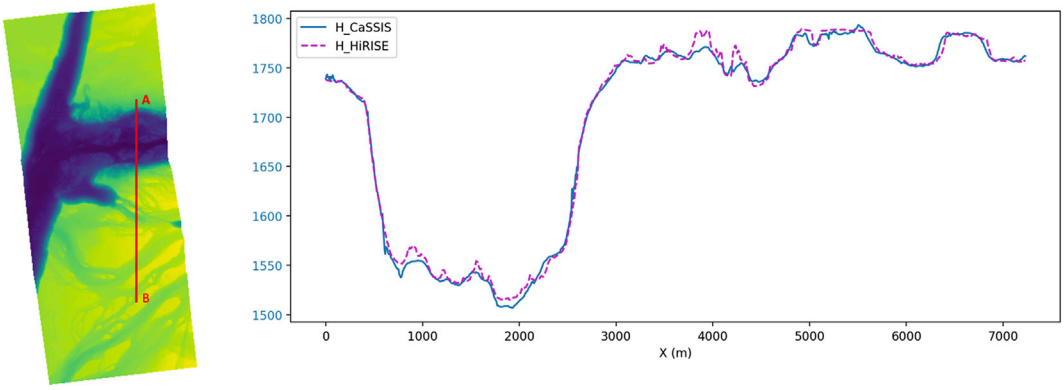

Fig. 19. Section extracted in Jovis Fossae (in red) on the left side and the corresponding profiles extracted from a CaSSIS DTM (affine T23) in blue and the HiRISE DTM in dotted magenta on the right.

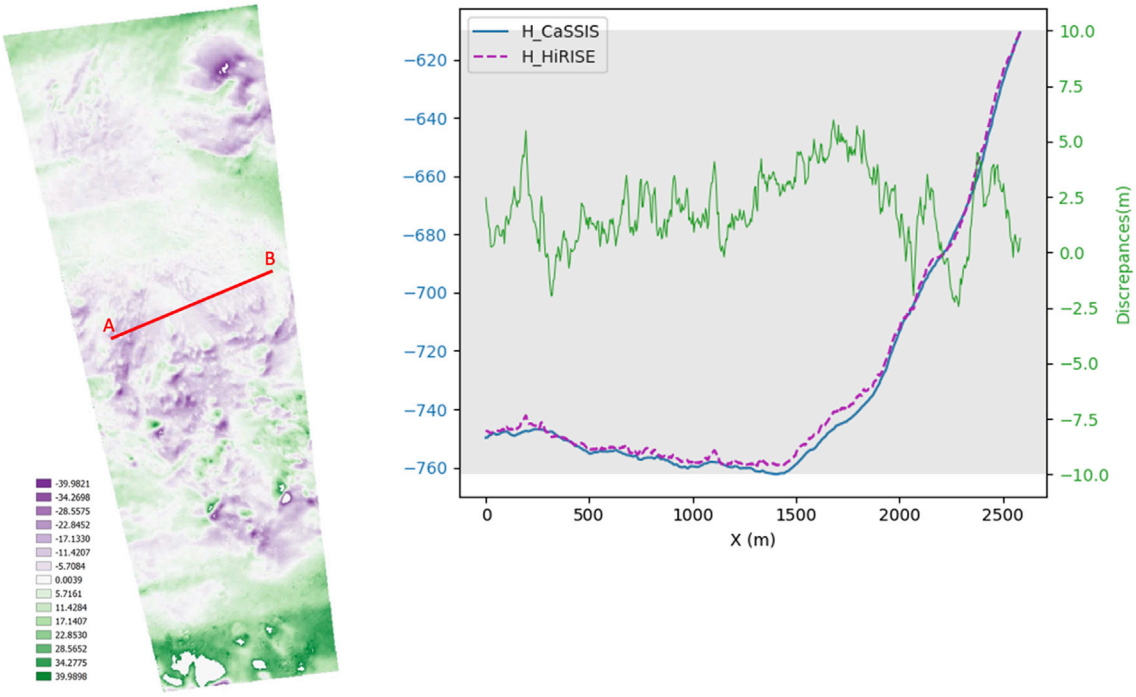

Fig. 20. On the left, the "Central Peak" DTM derived from the CaSSIS images and the discrepancies map derived in the overlapping region with the HiRISE DTM. In red the section extracted. On the right, the correspondent profiles extracted from the CaSSIS DTMs in blue, the HiRISE DTM in magenta and the plot of the differences between the two DTMs in green.

$$u(x,y) = \sum_{j=0}^{n}\sum_{i=0}^{j} a_{ij}x^{j-1}y^{i};\quad v(x,y) = \sum_{j=0}^{n}\sum_{i=0}^{j} bx^{j-1}y^{i} \qquad \text{(Equation 3)}$$

(Bethmann and Luhmann, 2011) and many other authors (Bruck et al., 1989) (Lu and Cary, 2000) (Re et al., 2014)showed that using different shape functions to model the geometric transformation in LSM can bring higher accuracy and solve, in some cases, numerical problems like pixel-locking which produces artificially peaked histograms of sub-pixel disparity.

These peaks correspond to the introduction of erroneous ripples or waves in the 3D reconstruction of truly flat surfaces (Stein and Matthies, 2006). At the same time, still according to (Bethmann and Luhmann, 2011), for high accuracy applications the type of geometric model, the texture of the image and the maximum curvature of the object surface have been taken into account in order to select the most useful configuration. The key to successful matching, as expressed in (Gruen, 2012), is an appropriate matching strategy, making use of all available and explicit knowledge concerning the sensor model, stereo-block structure and image content. Selection of correct matching parameters can be challenging to automate, because the requirements for these parameter values are often conflicting and as already mentioned, the matching parameters are functions of many factors, including terrain type, image texture, image scale, disparity variations and image noise.

The tests performed have the goal to identify the optimal size of the template as this parameter has a direct effect on the accuracy of the point measurement.

In general, with larger window sizes, the object details are reduced (with the typical effect of a low pass filtering) as also described in (Otto, 1989) but, on the other hand, they will produce less noisy matching results with lower correlation error. The "smoothing" effect is caused by the fact that the areas of the matching algorithm are assumed to correspond through the chosen transformation model for small surface patches: along small objects or edges, this assumption is not valid anymore and the surface average position (i.e. the position of the interpolating plane) is computed. At the same time, smaller image patches

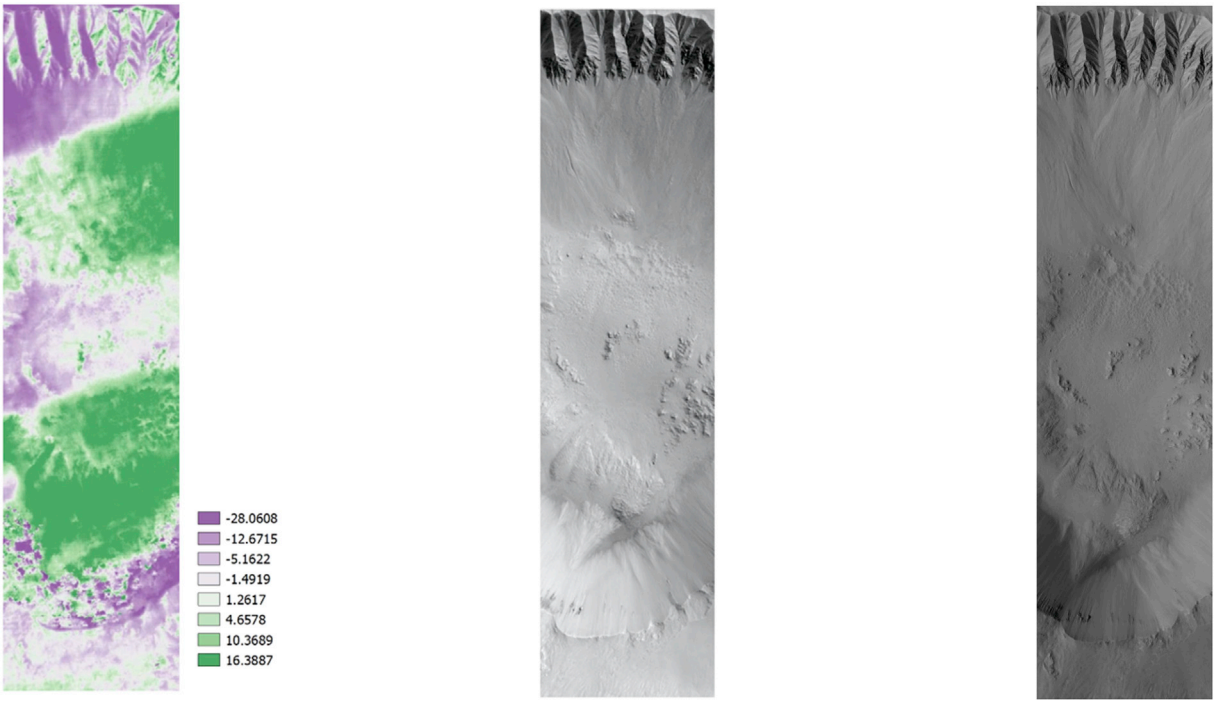

Fig. 21. Left side: Colour map of the discrepancies between CaSSIS and HiRISE "Gasa" DTMs, Middle: cropped CaSSIS image, Right side: cropped HiRISE image.

could theoretically reduce the smoothing effects, but may not be suitable for the correct determination of the matching reshaping parameters, because a small patch may not include enough image signal content. To evaluate the smoothing effect in the tests three template sizes were used (15x15, 23x23 and 31x31 pixels).

In order to quantify the terrain shape characteristics, the surface roughness has been considered in the study as geomorphometric variable (Grohmann et al., 2011). The surface roughness, in fact, is the deviation from the mean/average local flat surface and is an expression of the variability of a topographic surface.

The index is computed for each point of the HiRISE reference model (ground truth) and the values have been extracted by applying a least squares plane fitting interpolation to the points of the cloud within a sphere of fixed radius. The statistics of the surface roughness applied to all the four regions are reported revealing the morphologic differences for each region considered (Table 4 and in Fig. 17 the correspondent color coded maps.) The global characterization of the regions provides indications about the topographic variability of the surface for each terrain unit.

As presented in Table 4, by comparing the standard deviation values for each region, it emerges that "Hebes Chasma" and "Hale" are characterized by a higher overall roughness with respect to the "Central Peak" region characterized by the lowest global roughness. Considering the observations about the local contrast, we could hypothesize that the local contrast is mainly due to the composition variability and not to the morphology.

6. DTMs evaluation method and Co-registration

Regarding the DTM evaluation, an ideal reference dataset should be available in order to investigate the quality measures. In particular, the reference DTM should be independent with respect to the DTM to be assessed and preferably with higher precision.

Since in the planetary context, the ground control points are not available as on the Earth, the quality of the 3D reconstruction of the planetary surfaces must analyze internal consistency and comparisons with complementary remote sensing data (Oberst et al., 2014). Laser altimeter data are reliable reference data for stereo-photogrammetry but the comparisons are only useful when the laser footprint and the sampling distance along the tracks are comparable to the stereo ground sample distance (GSD).

The large differences in resolution between the MOLA data and CaSSIS suggest performing intercomparison of different stereo DTMs with similar resolutions that can also provide information about the consistency of the DTMs involved. The DTMs used as reference should be better in resolution and precision and must not contain internal distortions. In this context, the HiRISE DTMs, produced by the University of Arizona team over a period of several years, with GSDs of 1m or 2m (McEwen et al., 2010) are ideal references for a slightly lower resolution camera such as CaSSIS.

To extract robust statistics removed from overall systematic biasses and since the absolute accuracy is not considered in this context, a co-registration procedure on the DTMs has been applied. Starting with the removal of the main inconsistencies through a horizontal and vertical manual alignment in a Geographic Information System (GIS) environment with the selection of multiple corresponding points, a refinement in the registration has then been performed by a Least Squares (Koch, 1987) procedure though a dedicated tool. The process consists of extracting the differences on a uniform spatial distribution within the overlapping area of the two DTMs to co-register. The best solution for the registration of the two surfaces (the HiRISE reference DTM (already controlled to the MOLA data) and the second one on which we want to apply the correction (CaSSIS)) is achieved by minimizing a goal function that measures the elevation differences between the two surfaces.

A second method for the registration of the surfaces involved in the comparisons has been also applied for a further alignment refinement. The process consists in removing all the systematic inconsistencies and performing a best-fit automatic alignment through an iterative closest point (ICP) algorithm (Besl and Neil, 1992) already implemented in a 3D modelling software able to manage the DTMs converted to a triangulated irregular network (TIN) or point clouds format. The registration procedure performs only a rigid transformation and no warping. The procedure starts with a point-to-surface alignment to register the two datasets, then the iterative ICP alignment process is run to finally analyze

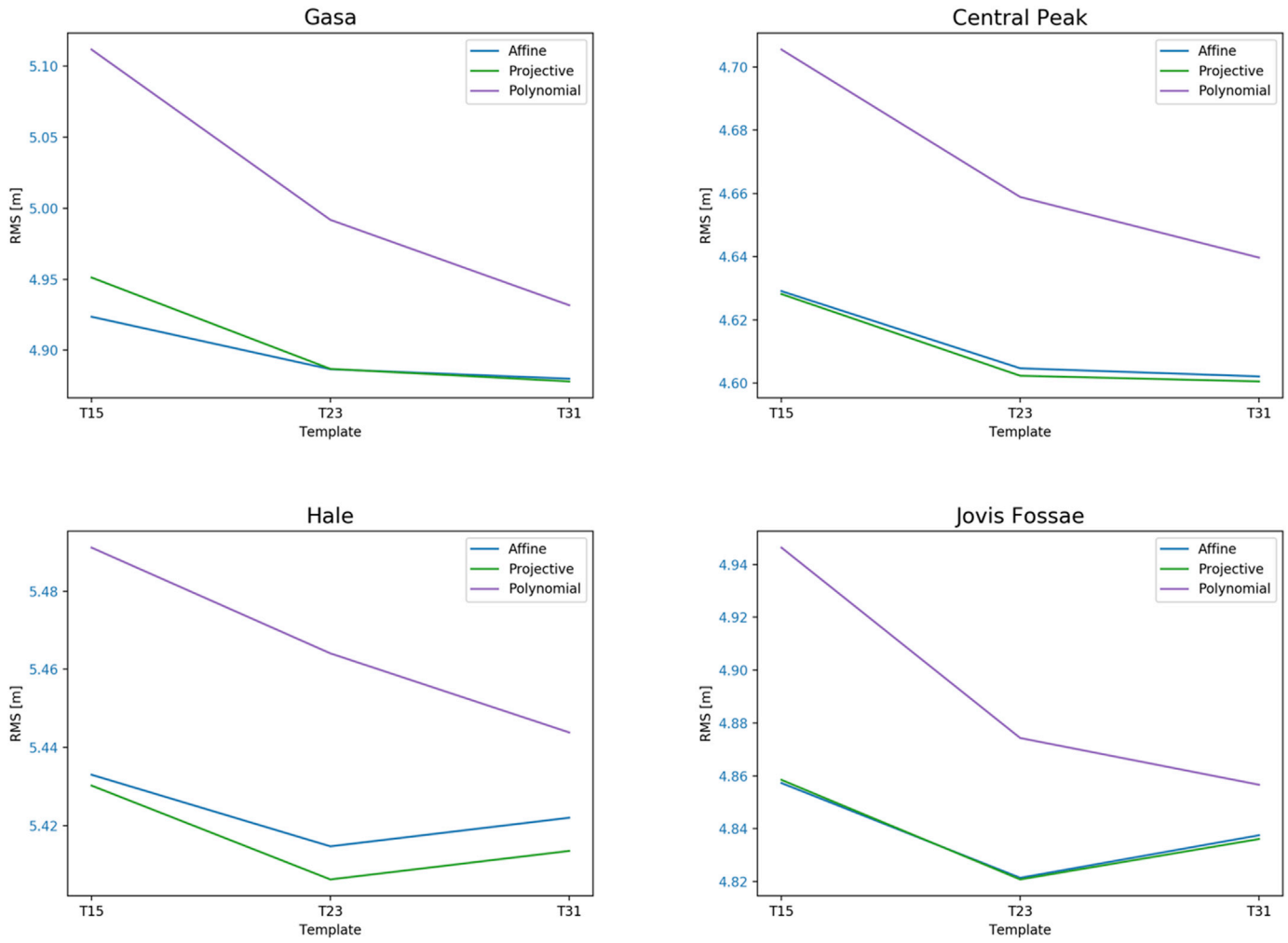

Fig. 22. For each region, the RMS of the differences between the CaSSIS DTMs and the HiRISE reference DTM have been plotted varying the Template sizes (15x15, 23x23, 31x31) and the shape models implemented in the Least Squares Matching algorithm.

only the differences in shape. All the DTMs involved in the comparison were previously converted to a TIN (Triangulated Irregular Network) representation, then, the signed distance of each triangulated surface from the reference one is computed. Due to the preliminary point-to-surface alignment, the average error is almost zero and therefore the Root Mean Square Error (RMSE) is close to the standard deviation of the discrepancies (Re et al., 2019).

After the co-registration process, the DTM evaluation is based on generating pair-wise height differences and analysing statistically the discrepancy maps (the RMSE have been computed). The approach for the quality evaluation starts with down-sampling the reference to the same GSD of the target DTM before computing the discrepancies. The availability of reference data of high quality such as the HiRISE DTMs is crucial for the testing and optimisation of the matcher performance as well as identifying the processing parameter tuning for optimisation. The Expected vertical Precision (EP) can be also evaluated from the theoretical formula as quantitative DTM assessment which can be approximated (Kirk et al., 2003; Simioni et al., 2021) to:

$$EP = \sigma_P \, p \, \frac{H}{c} \, \frac{H}{B} \qquad \text{(Equation4)}$$

where H (height) is the height of the centre of perspective, c is the focal length, p the pixel pitch, the H/B (baseline) ratio is calculated from the three-dimensional intersection geometry, and σ_P is the RMS stereo-matching error in pixel units (0.2–0.3 pixel often used as a rule of thumb (Cook et al., 1996 and Otto et al., 1989).

The results for each region are reported in Table 5.

6.1. Comparisons

From the comparisons between the CaSSIS DTMs and the HiRISE DTMs used as reference, the statistics (Standard Deviations (STD) and Root Mean Square Errors (RMSE)) of the pair-wise height differences between the 3D models provide important indications about the quality of the 3DPD results.

The standard deviations of the four comparison datasets, computed over the whole overlapping areas are presented in Table 6 and the corresponding coloured maps in Fig. 18.

The values appear quite larger than those expected from the EP values reported in Table 5. The results reflect the fact that the comparison involves all the 3D points generated (no correlation threshold has been applied that removes the highest matching inconsistencies (outliers), differently from the nominal approach of the pipeline which removes the matching points with low fidelity with low values of NCC). This means that obvious bias effects associated with framelets borders or shifts have been included in the statistical computation. Of course, many improvements will be applied in the future, especially after the implementation of bundle adjustment procedures for the mitigation of the residual coalignment errors between framelets.

In Fig. 19, we have extracted the profiles from the CaSSIS and HiRISE DTMs of "Jovis Fossae" to investigate the details of the topographic

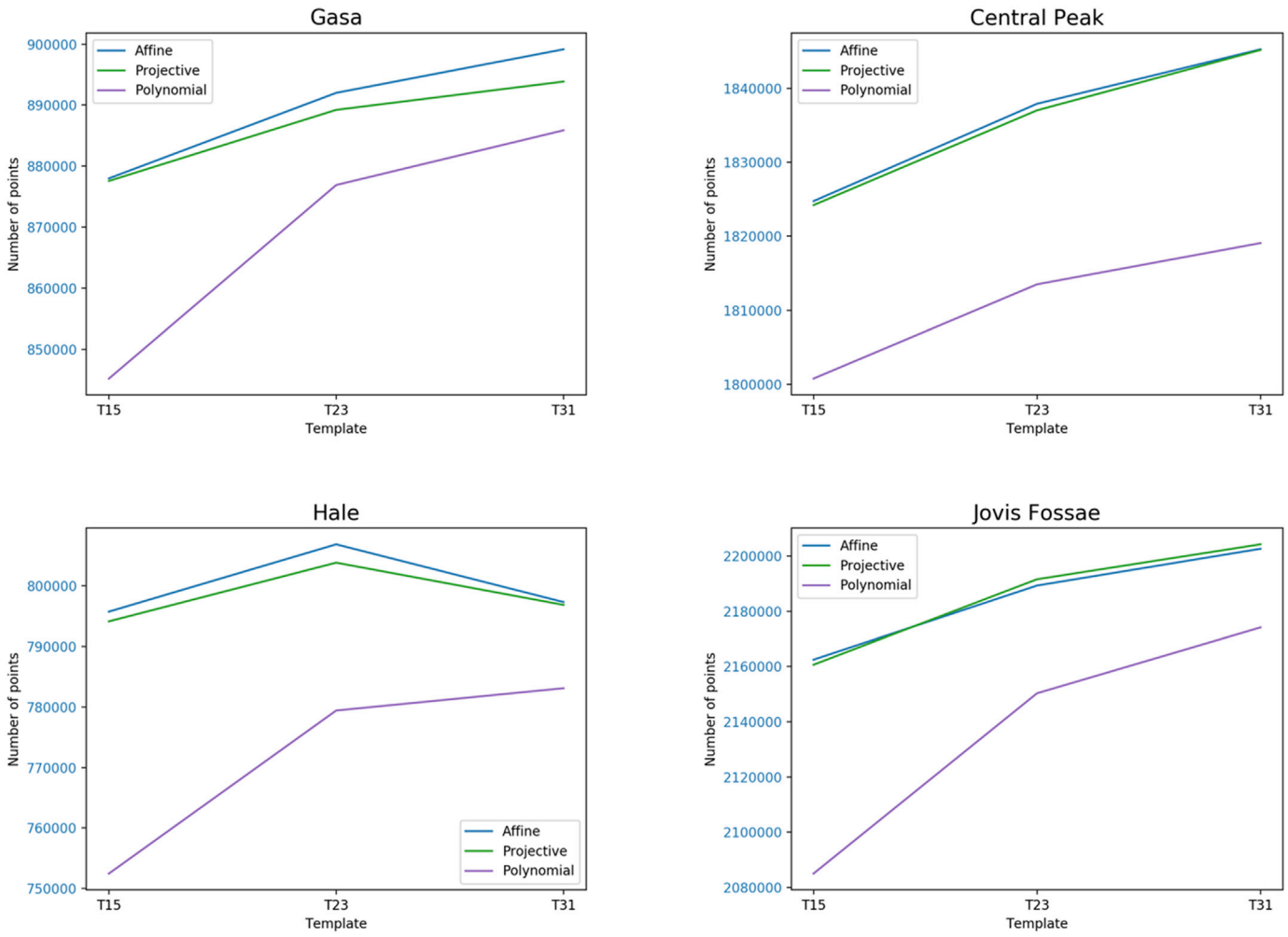

Fig. 23. For each region, the number of points considered in the comparisons between the CaSSIS DTMs and the HiRISE reference DTM have been plotted varying the Template sizes (15x15, 23x23, 31x31) and the shape models implemented in the Least Squares Matching algorithm.

results, confirming the good agreement between the two datasets after the co-registration procedure. The profiles are well aligned even though, at some small ranges the distances improve, especially in correspondence of some curvature changes. The same observations can be done for the "Central Peak" reported in Fig. 20 where the discrepancies between the two DTMs are also plotted and appear quite small especially within a single framelet region. At the same time, the discrepancy map reveals in some areas the "jitter effect" introduced in the mosaicking process that reflects a slight misalignment between the framelets during the composition of the whole image.

What can be noticed in Fig. 21 is that the shadows on the HiRISE images reflect the distribution of the discrepancies among the surface highlighting the influence of the illumination on the reconstruction (especially looking at the gullies on the crater rim).

In Fig. 22, for each area of interest, the RMSE of the differences and the number of points involved in the comparisons (Fig. 23) have been plotted varying the template sizes for each of the shape models implemented in the Least Squares matching process.

It is important to highlight that for this comparison procedure a threshold of $\pm$ 10 m has been applied to the differences in order to reject the outliers (especially the points on the borders located between the framelets) from the analysis and derive considerations only from the robust matched points involved.

The definition of a threshold for considering robust matching points can be applied directly at the correlation phase, rejecting the points as function of the Normalized Cross Correlation (NCC) coefficient that determines the Quality Map (Lewis, 1995). In our procedure, we applied the filtering of the outliers at the final stage, at the comparison step. The RMSE results reported in the plots (Fig. 22), just because of the threshold applied, lower the values and reduce the number of points considered in the comparison. This choice has been defined in order to precisely consider only the more robust matching points.

What emerges from the analisys (Figs. 22 and 23) is that the RMS error of the discrepancies, considered as a proxy of the elevation accuracy of the DTMs under evaluation, improves with the template sizes independently from the shape model for the first two cases (" Gasa" and "Central Peak"). For the last two regions ("Hale" and "Jovis Fossae") instead, the behavior of the RMS error with the template size is different for the polynomial function with respect to the affine and projective models. The polynomial shape function seems to describe the terrain better with large template sizes while the affine and the projective reach a minimum for the template 23x23. For all the regions, the homography and the affine shapes always provide better results. In addition, the number of points involved in the comparisons are important to be analyzed in all cases; in Fig. 23, the polynomial function provide a lower number of points to be compared with respect to the other two functional models combined with lower RMS values for all the settings. This behavior is also confirmed on the graph shown in Fig. 24. The Polynomial function in fact, deviates from the other profiles in multiple ranges.

For the case of the Hebes Chasma region where the HiRISE stereo pairs are not available, the comparisons have also been performed between the CaSSIS and CTX datasets. This area is characterised by strong

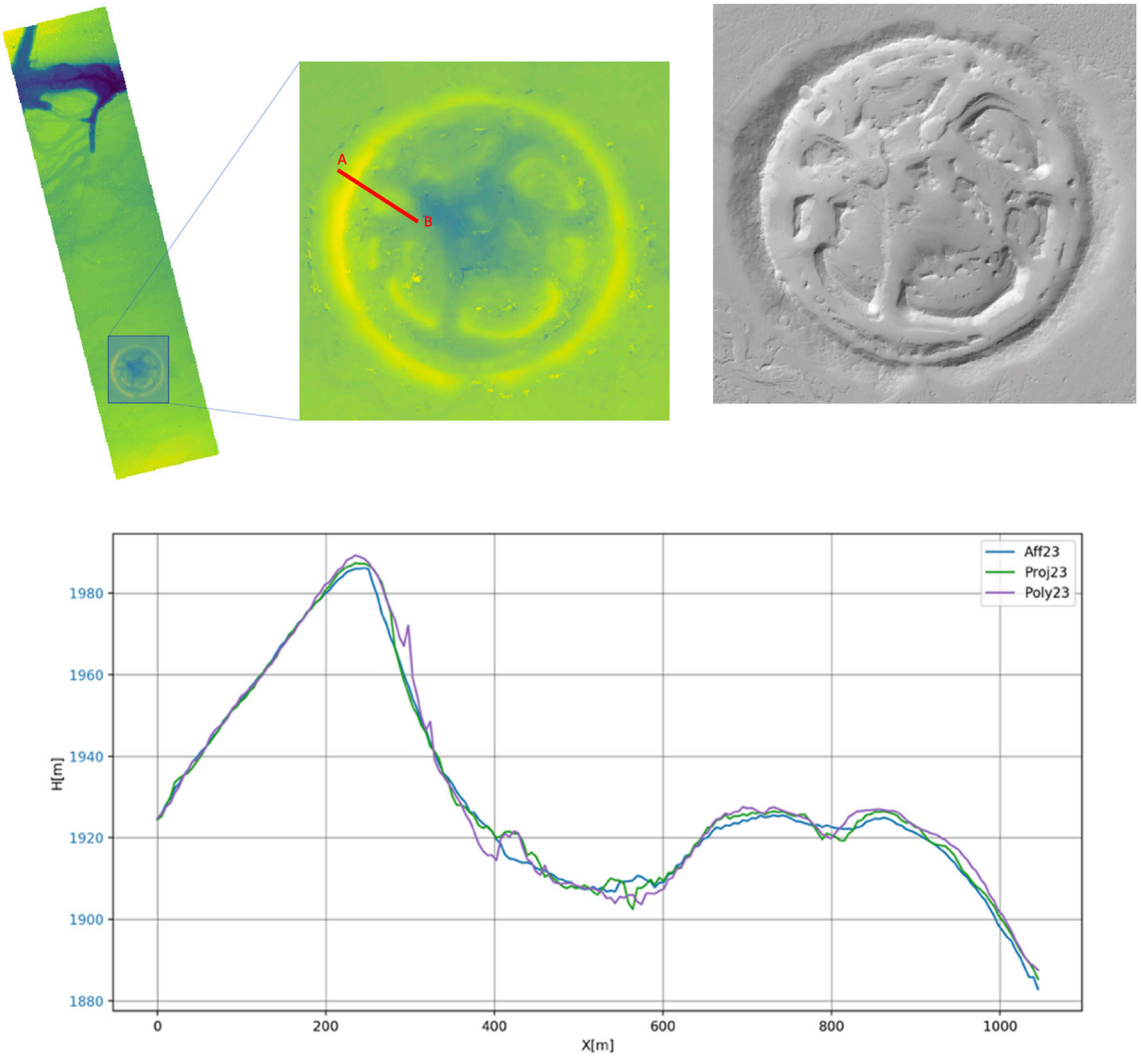

Fig. 24. On the top left, section extracted in Jovis Fossae (in red) and bottom; on the top right, the image of the experimental area and on the bottom, the correspondent profiles extracted from the CaSSIS DTMs generated applying the affine shape model in green, the projective transformation in blue and the polynomial transformation in purple. The template size has been fixed to 23x23 pixels.

morphologic complexity and at the end of the co-registration procedure, the DTMs produced from CaSSIS and CTX do not provide good correspondences.

The map of the discrepancies reveals high STD values (38.93 m). Fig. 25 shows a section profile where the two surfaces are compared.

To further evaluate the performance of the 3DPD pipeline, a qualitative assessment has been also applied to the DTMs generated in the experiment. In particular, a visual examination of the shaded relief versions of the DTM (Fig. 26 and Fig. 27) obtained with different template sizes emphasizes the details of the surface and suggests the smoothing effect of enlarging the size of the matching window.

The differences between the CaSSIS and HiRISE images of "Jovis Fossae" in Fig. 27(a and b) are due to the difference of image resolution (4.6 m vs 25 cm) and the different illumination conditions (incidence angle).

Looking at the shaded relief views of the Jovis Fossae region DTMs generated by applying the three different shape models (Fig. 27), the appearance of the DTMs looks more complex with the increase of the degree of the transformation. The polynomial shape models, especially looking at Fig. 27, reveal a clear difference with the products obtained with the affine and the projective models (quite similar to each other). The Polynomial transformation instead, seems to generate DTMs characterized by some kind of fluctuations on the surface that are hardly discernible and definable as noise or real small size details of the surface features.

In any case, the smoothing effect introduced by the enlarging of the template size is also evident.

In Fig. 27, the hillshade of the HiRISE DTM (c) can be directly compared to the CaSSIS terrain shaded relief revealing immediately the higher capability of HiRISE to resolve the individual "small" features on the terrain, primarily for the highest spatial resolution. Then, the 3DPD products show some contouring artifacts especially along the steep slopes and as well as the evident blunders that decrease in abundance with the increasing of the template size. It is worth noting that the CaSSIS DTMs have been generated without applying any blunder filter based, for instance, on the matching quality threshold nor post-processing smoothing have been applied. Consequently the appearance of the terrain shaded relief could be quite noisy in the examples of Fig. 27 as for Figs. 6–8-10 and 14. In this context, we followed this strategy to have a stronger control on the impact of the setting parameters through the matching algorithm. The nominal pipeline approach foresees to avoid these artifacts by applying a region growing filtering followed by filling holes through an interpolation process.

In Fig. 12 is more evident, instead, the jitter-like effect is more

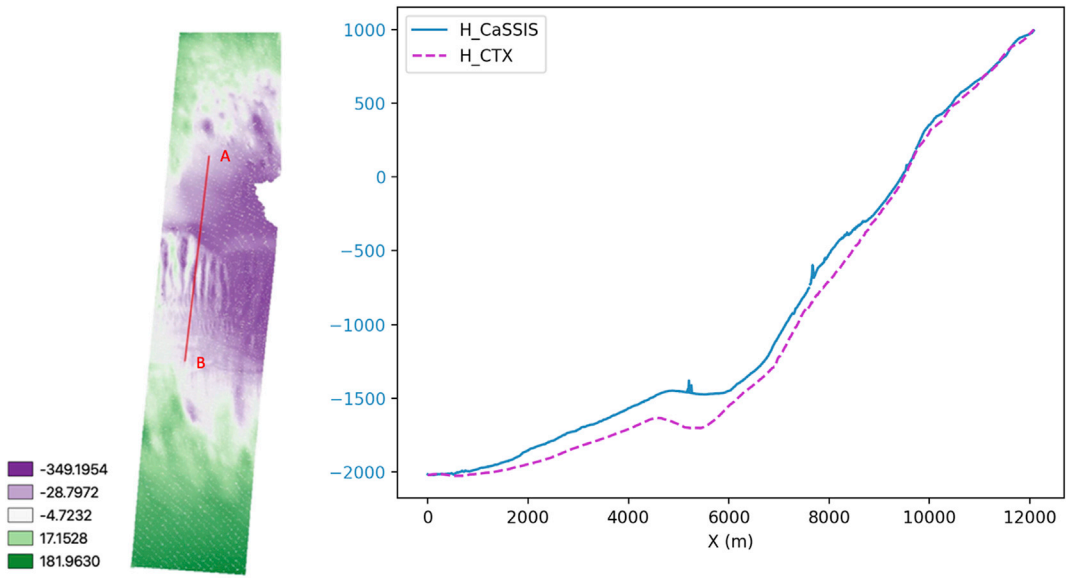

Fig. 25. On the left, the discrepancies map derived from the differences between the CaSSIS DTM and the CTX DTM. In red, the section extracted. On the right, the correspondent profiles extracted from the two surfaces co-registered.

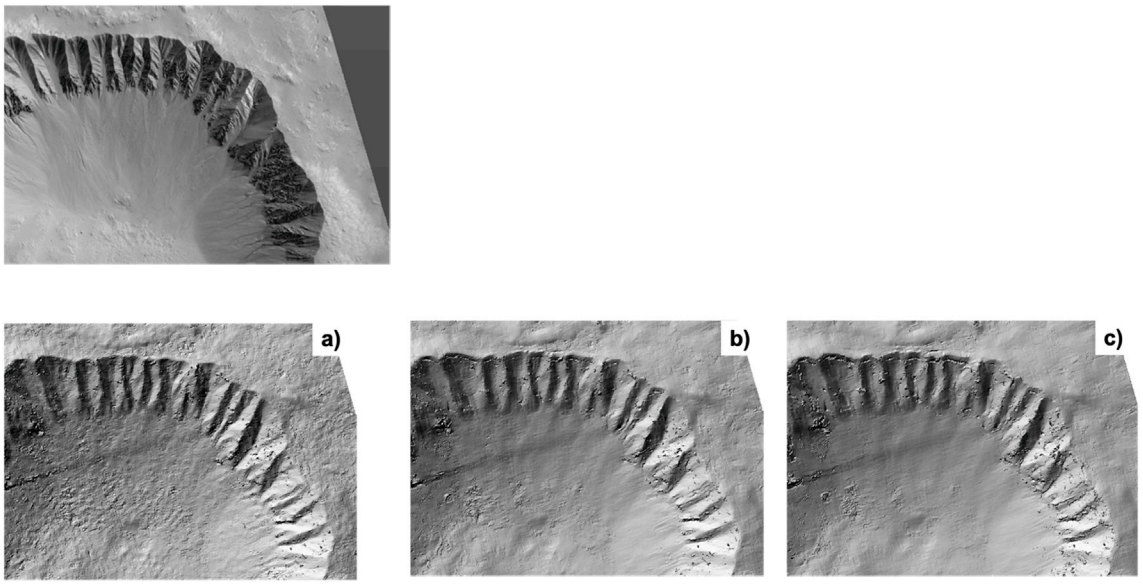

Fig. 26. Gasa region - CaSSIS Image on the top, DTM Hillshade version for a) T15, b) T23, c) T31.

evident, likely having been introduced during the mosaicking process that combine the single framelets of the CaSSIS sequence acquisition. The pointing kernels may not be capturing the higher frequencies of spacecraft motion, causing slight misalignments of framelets during the initial mosaicking stage, resulting visible steps in the DTM at framelet boundaries. Some procedures of de-jittering have been investigated but not examined in this context.

7. Summary and conclusions

This work provides a review of the CaSSIS stereo products supported by a description of the applied methods and examines the correlation between the quality of the images in terms of image content and the topographic characteristics with the matching performance that directly affects the quality of DTMs.

Excluding from the discussion the "Hebes Chasma" area that misses the HiRISE reference model (and the derived RMSE of the discrepancies), even though the aim of the paper does not foresee going deeply into the absolute accuracy of the CaSSIS stereo products, the statistics obtained from the comparisons suggested that "Jovis" and "Central Peak" have provided the best results, while the "Hale" case on the contrary has produced the highest STD values. In the latter case, the poorer matching performances are not unexpected considering the strong complexity of the terrain that, especially in the areas characterised by the RSL features, presents several discontinuities and changes in roughness and slopes. Lower RMSE values are encountered with the "Central Peak" and "Jovis Fossae" cases while "Hale" provides lower accuracy values (Fig. 22). The high agreement between "Jovis Fossae" and "Central Peak" areas and the reference HiRISE DTMs can be also facilitated by the gentle slope of the area. The matching process, beyond the improvement derived from the good image quality, could be also favoured by the light slopes preserved from strong changes in perspective that could make difficult the homologous point identification. From these considerations, some indications about the optimisation of the matching process can be

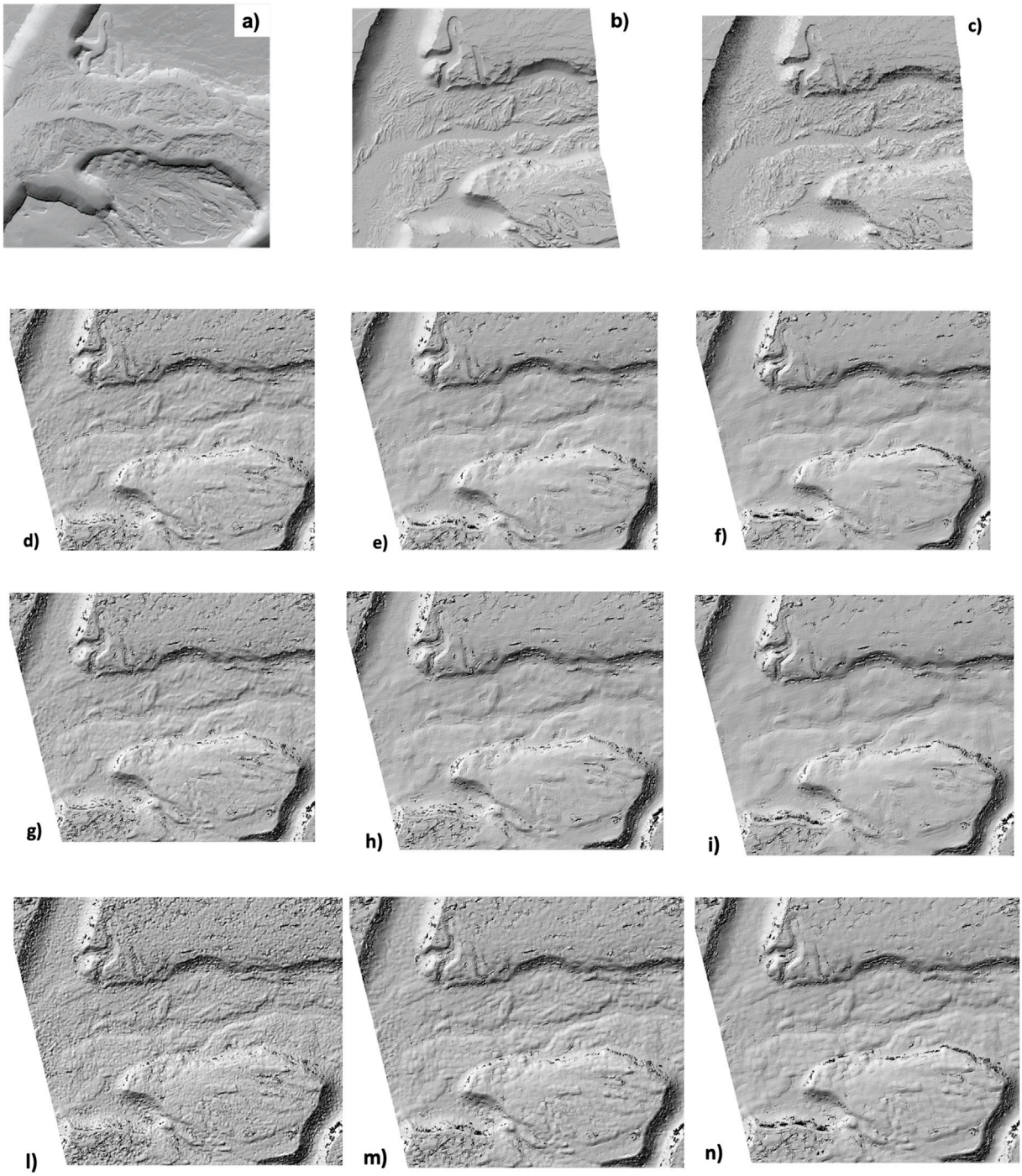

Fig. 27. Jovis Fossae region – a) CaSSIS image, b) HiRISE image, c) Hillshade version of HiRISE DTM and the Hillshade versions of DTMs obtained with: d) Affine model T15, e) Affine model T23, f) Affine model T31, g) Projective model T15, h) Projective model T23, i) Projective model T31, l) Polynomial model T15, m) Polynomial model T23, n) Polynomial model T31.

extrapolated.

Taken together, the image quality (i.e, local contrast, illumination, noise) and the morphological properties of the terrain could suggest the best combination of parameters. Where a steep slope is present or a fine edge such as the contour of a crater rim or along the gullies (as in the "Gasa" region), we intend to extract as much detail as possible, avoiding the smoothing effect introduced by a big template size. On the contrary, on a flat or very gentle slope on a region already intrinsically smooth (as big extensions in "Hale" or "Jovis Fossae"), the use of larger template sizes can be useless. In general, from the experience gained over the three years of DTM generation with the 3DPD pipeline, the best results were achieved in the cases of areas with a significant terrain relief and optimum lighting conditions. These conditions mean that the contrast between the shaded and lit areas is not extreme. Mild to strong contrast is optimum, especially in case of large, preferably even slopes (with features visible despite a deep shade). The solar incidence angle was not deeply analyzed in this context, but it is crucial for the effect. Holes appeared mainly on crater rims, where shaded or brightly lit parts were sometimes out of contrast range and features were not recorded on the source image. In some cases, the features were recorded on the source image, but not registered by the algorithm. In those cases, a human user could match the features manually, either objectively or arbitrarily (in

the second case to avoid a hole in the DTM, although with a loss of information). Relatively flat areas did return good DTM products, as long as the image was sharp and lighting conditions were optimum to capture either the texture or small features (usually craters). The best results for flat terrain were achieved if a DTM included at least one very distinctive relief feature (such as a valley cutting through the plain). A good example of a flat terrain with distinctive features is "Jovis Fossae".

The stereo products generated so far and compared with HiRISE reference DTMs provide several indications for the identification of the right configuration for an optimal stereo processing.

Clearly, other comparisons with hight resolution CaSSIS DTMs could lead to further improvements. A valuable example is the recent deep learning based DTM estimation system that produces a full-strip CaSSIS DTM described in (Tao et al., 2021), or the combination of shape-from-shading with super-resolution CaSSIS images to generate 1m GSD DTMs (Tao et al., 2021).

In conclusion, the strengths of the 3DPD pipeline are the possibility to access to the matching core and the tunable processing parameters which have proved to be extremely promising and also opens towards several future works and tests for the performance analysis and for the definition of new strategies based on the scientific cases, for instance. Furthermore, the online repository (https://cassis.oapd.inaf.it/archive) that collects all the stereo products produced by the team at OAPD can be considered valuable for the dissemination to the scientific community.

Author statement

C. Re: Conceptualization, Methodology, Software, Formal analysis, Investigation, Writing - Original Draft, Writing - Review & Editing, Visualization, Supervision.

A. Fennema: Software, Data Curation, Metodology, Writing - Review & Editing.

E. Simioni: Software, Data Curation, Visualization, Supervision.

S. Sutton: Review & Editing, Supervision.

D. Mège: Writing, Metodology, Visualization.

K. Gwinner: Supervision.

M. Józefowicz: Resources.

G. Munaretto: Resources.

M. Pajola: Editing.

A. Petrella: Data Curation.

A. Pommerol: Data Curation.

G. Cremonese: Project administration, Funding acquisition.

N. Thomas: Funding acquisition, Supervision.

Declaration of competing interest

The authors declare that they have no known competing financial interests or personal relationships that could have appeared to influence the work reported in this paper.

Acknowledgements

CaSSIS is a project of the University of Bern and funded through the Swiss Space Office via ESA's PRODEX programme. The instrument hardware development was also supported by the Italian Space Agency (ASI) (ASI-INAF agreement no. 2020-17-HH.0), INAF/Astronomical Observatory of Padova, and the Space Research Center (CBK) in Warsaw. Support from SGF (Budapest), the University of Arizona (Lunar and Planetary Laboratory) and NASA are also gratefully acknowledged. Operations support from the UK Space Agency under grant ST/R003025/1 is also acknowledged. CTX DTMs were generated using the MarsSI (marssi.univ-lyon1.fr) (Poulet et al., 2018) application founded by the European Union's Seventh Framework Program (FP7/2007–2013) (ERC Grant Agreement No. 280168). Some of the CaSSIS DTMs were generated within the framework of the EXOMHYDR project, carried out within the TEAM programme of the Foundation for Polish Science co-financed by the European Union under the European Regional Development Fund.

Appendix A. Supplementary data

Supplementary data to this article can be found online at https://doi.org/10.1016/j.pss.2022.105515.

References

Acton Jr., C.H., 1996. Ancillary data services of NASA's navigation and ancillary information facility. Planet. Space Sci. 44 (1), 65–70.

Bay, H., Ess, A., Tuytelaars, T., Van Gool, L., 2008. Speeded-up robust features (SURF). Comput. Vis. Image Understand. 110 (3), 346–359.

Becerra, P., Sori, M.M., Thomas, N., Pommerol, A., Simioni, E., Sutton, S.S., et al., 2019. Timescales of the climate record in the south polar ice cap of Mars. Geophys. Res. Lett. 46, 7268–7277.

Beyer, R.A., Alexandrov, O., McMichael, S., 2018. The Ames Stereo Pipeline: NASA's open source software for deriving and processing terrain data. Earth Space Sci. 5 (9), 537–548.

Becker, K., Becker, T., Berry, K.L., Edmundson, K.L., Goins, A., Wilson, T.J., 2018. Updates to integrated software for imagers and Spectrometers. In: Lunar and Planetary Science Conference, p. 3007, 2083.

Besl, P.J., Neil, D.M., 1992. Method for Registration of 3-D Shapes. Sensor Fusion IV: Control Paradigms and Data Structures, vol. 1611. International Society for Optics and Photonics.

Bethmann, F., Luhmann, T., 2011. Least-squares matching with advanced geometric transformation models. Photogramm. Fernerkund. GeoInf. 57–69.

Bruck, H.A., McNeill, S., Sutton, M.A., Peters III, M.H., 1989. Digital image correlation using Newton-Raphson method of partial differential correction. Exp. Mech. 29, 261–267.

Cook, A., Oberst, J., Roatsch, T., Jaumann, R., Acton, C., 1996. Clementine imagery: selenographic coverage for cartographic and scientific use. Planet. Space Sci. 144 (10), 1135–1148.

Cremonese, G., Re, C., Simioni, E., Mudric, T., Petrella, A., Thomas, N., 2018. The CaSSIS Digital Terrain Model Generation and Archiving at OAPD. EPSC abstract.

Delamere, W.A., Tornabene, L.L., McEwen, A.S., Becker, K., Bergstrom, J.W., Bridges, N.T., Thomas, N., 2010. Color imaging of Mars by the high resolution imaging science experiment (HiRISE). Icarus 205 (1), 38–52.

Grohmann, C.H., Smith, M.J., Riccomini, C., 2011. Multi-scale Analysis of topographic surface roughness in the midland valley, Scotland. IEEE Trans. Geosci. Rem. Sens. 49, 1200–1213.

Gruen, A., 1985. Adaptive least squares correlation: a powerfulimage matching technique. South African J. Photog. Rem. Sens. Cartog. 14 (3), 175–187.

Gruen, A., 2012. Development and status of image matching in photogrammetry. Photogramm. Rec. 27, 36–57.

Gwinner, K., Scholten, F., Spiegel, M., Schmidt, R., Giese, B., Oberst, J., Neukum, G., 2009. Derivation and validation of high-resolution digital terrain models from Mars Express HRSC data. Photogramm. Eng. Rem. Sens. 75 (9), 1127–1142.

Jaumann, R., Neukum, G., Behnke, T., Duxbury, T.C., Eichentopf, K., Flohrer, J., Hoffmann, H., 2007. The high-resolution stereo camera (HRSC) experiment on Mars Express: instrument aspects and experiment conduct from interplanetary cruise through the nominal mission. Planet. Space Sci. 928–952.

Kirk, R., Howington-Kraus, E., Redding, B.L., Galuszka, D.M., Hare, T.M., Archinal, B.A., Barrett, J.M., 2003. High-resolution topomapping of candidate MER landing sites with Mars Orbiter Camera narrow-angle images. J. Geophys. Res.: Planets 108 (E12).

Kirk, R.L., Fergason, R.L., Redding, B., Galuszka, D., Smith, E., Mayer, D., Gwinner, K., 2020. Evaluating stereo DTM quality at jezero crater, Mars with HRSC, CTX, and HiRISE images. Int. Arch. Photogram. Rem. Sens. Spatial Inf. Sci. 43, 1129–1136.

Kirk, R.L., Howington-Kraus, E., Rosiek, M.R., Anderson, J.A., Archinal, B.A., Becker, K.J., McEwen, A.S., 2008. Ultrahigh resolution topographic mapping of Mars with MRO HiRISE stereo images: meter-scale slopes of candidate Phoenix landing sites. J. Geophys. Res.: Planets 113 (E3).

Koch, K.R., 1987. Parameter Estimation and Hypothesis Testing in Linear Models. Springer Verlag.

Kolb, K.J., Pelletier, J.D., McEwen, A.S., 2010. Modeling the formation of bright slope deposits associated with gullies in Hale Crater, Mars: implications for recent liquid water. Icarus 205 (1), 113–137.

Lewis, J., 1995. Fast normalized cross-correlation. Proc. Vision Interf. 120–123.

Lu, H., Cary, P., 2000. Deformation measurements by digital image correlation: implementation of a second-order displacement gradient. Exp. Mech. 40, 393–400.

Malin, M.C., Bell, J.F., Cantor, B.A., Caplinger, M.A., Calvin, W.M., Clancy, R.T., Lee, S.W., 2007. Context camera investigation on board the Mars reconnaissance orbiter. J. Geophys. Res.: Planets 112.

McEwen, A.S., Banks, M.E., Baugh, N., Becker, K., Boyd, A., Bergstrom, J.W., Wray, J.J., 2010. The high resolution imaging science experiment (HiRISE) during MRO's primary science phase (PSP). Icarus 205 (1), 2–37.

McEwen, A.S., Eliason, E.M., Bergstrom, J.W., Bridges, N.T., Hansen, C.J., Delamere, W.A., Kirk, R.L., 2007. Mars reconnaissance orbiter's high resolution imaging science experiment (HiRISE). J. Geophys. Res.: Planets 112 (E5).

McEwen, A.S., Ojha, L., Dundas, C.M., Mattson, S.S., Byrne, S., Wray, J.J., Gulick, V.C., 2011. Seasonal flows on warm Martian slopes. science. Science 333 (6043), 740–743.

Miller, S.B., Walker, A.S., 1993. Further developments of Leica digital photogrammetric systems by Helava. Acsm Asprs Annual Convention 3, 256-256.
Mouginis-Mark, P.J., 1990. Recent water release in the Tharsis region of Mars. Icarus 84 (2), 362–373.
Munaretto, G., Pajola, M., Cremonese, G., Re, C., Lucchetti, A., Simioni, E., Massironi, M., 2020. Implications for the origin and evolution of martian recurring slope lineae at Hale Crater from CaSSIS observations. Planet. Space Sci. 187.
Munaretto, G., Pajola, M., Lucchetti, A., Re, C., Cremonese, G., Simioni, E., Cambianica, P., Thomas, N., 2021. Topographic correction of HiRISE and CaSSIS images: validation and application to color observations of Martian albedo features. Planet. Space Sci. 200, 105198, 2021.
Neukum, G., Jaumann, R., 2004. HRSC: the high resolution stereo camera of Mars Express. Mars Express: Scientific Payload 1240, 17–35.
Oberst, J., Gwinner, K., Preusker, F., 2014. Exploration and analysis of planetary shape and topography using stereophotogrammetry. Encyc. Solar Syst. 1223–1233.
Okubo, C., Tornabene, L., Lanza, N.L., 2011. Constraints on mechanisms for the growth of gully alcoves in Gasa crater, Mars, from two-dimensional stability assessments of rock slopes. Icarus 211 (1), 207–221.
Otto Gp, C.T., 1989. Region-growing' algorithm for matching of terrain images. Image Vis Comput. 7 (2), 83–94.
Plescia, J., 2013. Olympica fossae, Mars: recent fluvial-volcanic activity. Eur. Planet. Sci. Congr.
Pommerol, A., 2021. In-flight photometric calibration of CaSSIS images. Planet. Space Sci. (Under review - this Issue).
Poulet, F., Quantin-Nataf, C., Ballans, H., Dassas, K., Audouard, J., Carter, J., Séjourné, A., 2018. PSUP: a planetary SUrface portal. Planet. Space Sci. 150, 2–8.
Re, C., Tulyakov, S., Simioni, E., Mudric, T., Cremonese, G., Thomas, N., 2019. Performance evaluation of 3DPD, the photogrammetric pipeline for the cassis stereo images. Int. Arch. Photogram. Rem. Sens. Spatial Inf. Sci. 42, 1443–1449.
Re, C., Roncella, R., Forlani, Cremonese, G., Naletto, G., 2014. Evaluation of an area-based matching algorithm with advanced shape models. Int. Arch. Photogram. Rem. Sens. Spatial Inf. Sci. XL-4, 215–221.
Schmidt, G., Fueten, F., Stesky, R., Flahaut, J., Hauber, E., 2018. Geology of Hebes Chasma, Mars: 1. Structure, stratigraphy, and mineralogy of the interior layered deposits. J. Geophys. Res.: Planets 123 (11), 2893–2919.
Schon, S.C., 2012. Gasa impact crater, Mars: very young gullies formed from impact into latitude-dependent mantle and debris-covered glacier deposits? Icarus 218 (1), 459–477.
Simioni, E., Re, C., Mudric, T., Cremonese, G., Tulyakov, S., Petrella, A., Thomas, N., 2021. 3DPD: a photogrammetric pipeline for push frame stereo cameras. Planet. Space Sci. 198.
Stein, A.H., Matthies, L., 2006. Attenuating stereo pixel-locking via affine window adaptation. IEEE Int. Conf. Robot. Auto. 914–921.
Tao, Y., Xiong, S., Conway, S., Muller, J.P., Guimpier, A., Fawdon, P., Cremonese, G., 2021a. Rapid single image-based DTM estimation from ExoMars TGO CaSSIS images using generative adversarial U-nets. Rem. Sens. 13 (15), 2877.
Tao, Y., Conway, S., Muller, J.P., Putri, A.R., Thomas, N., Cremonese, G., 2021b. Single image super-resolution restoration of TGO CaSSIS colour images: demonstration with perseverance rover landing site and Mars science targets. Rem. Sens. 13 (9), 1777.
Tanaka, K.L., Fortezzo, C.M., Skinner Jr., J.A., Hare, T.M., 2014. The digital global geologic map of Mars: chronostratigraphic ages, topographic and crater morphologic characteristics, and updated resurfacing history. Planet. Space Sci. 95, 11–24.
Thomas, N., 2021. CaSSIS Operation paper. Planet. Space Sci. (Under review- this Issue).
Thomas, N., Cremonese, G., Ziethe, R., Gerber, M., Brändli, M., Bruno, G., Gruber, M., 2017. The colour and stereo surface imaging system (CaSSIS) for the ExoMars trace gas orbiter. Space Sci. Rev. 1897–1944.
Tulyakov, S., Ivanov, A., Thomas, N., Roloff, V., Pommerol, A., Cremonese, G., Fleuret, F., 2018. Geometric calibration of colour and stereo surface imaging system of ESA's Trace Gas Orbiter. Adv. Space Res. 61 (1), 487–496.
Zhang, B., Miller, S., Walker, S., DeVenencia, K., 2007. Next generation automatic terrain extraction using Microsoft ultracam imagery. ASPS 2007 Annual Conference.